UNIVERSITY OF CALIFORNIA,
IRVINE

Applications of Laser Therapy for Anterior Cornea Drug Delivery and Treatment

DISSERTATION

submitted in partial satisfaction of the requirements
for the degree of

DOCTOR OF PHILOSOPHY

in Biomedical Engineering

by

Rohan Joshi

Dissertation Committee:

Professor James Jester, Chair

Professor Tibor Juhasz

Professor Eric Pearlman

2025

TABLE OF CONTENTS

LIST OF FIGURES

LIST OF TABLES

VITA

Rohan Joshi

2019 B.S. in Biomedical Engineering, Arizona State University

2019-25 Graduate Student Researcher, Department of Ophthalmology, University of California, Irvine

2024 M.S. in Biomedical Engineering, University of California, Irvine

2025 Ph.D. in Biomedical Engineering, University of California, Irvine

PUBLICATIONS

Joshi, R., Bradford, S. M., Luo, S., Farrah, E., Xie, Y., Brown, D. J., Juhasz, T., & Jester, J. V. (2025). Enhanced riboflavin stromal delivery using microchannel-assisted iontophoresis for corneal crosslinking. *Translational Vision Science & Technology*, 14(3), 18. https://doi.org/10.1167/tvst.14.3.18

CONFERENCES

Association for Research in Vision and Ophthalmology (ARVO) Conference, May 2023.
Poster Presentation: Enhanced Riboflavin Stromal Delivery Using Microchannel-Assisted Iontophoresis for Corneal Crosslinking

Association for Research in Vision and Ophthalmology (ARVO) Conference, May 2024.
Poster Presentation: Selective Photothermal Ablation (SPA) of Meibomian Glands Using a High Intensity 1726 nm Laser

Bench to Bedside Symposium, June 2023.
Poster Presentation: Enhanced Riboflavin Stromal Delivery Using Microchannel-Assisted Iontophoresis for Corneal Crosslinking

Bench to Bedside Symposium, June 2024.
Poster Presentation: Selective Photothermal Ablation (SPA) of Meibomian Glands Using a High Intensity 1726 nm Laser

ACKNOWLEDGEMENTS

This project would not have been possible without the constant support and encouragement from my advisor, Dr. James Jester. Not only did he keep me on track throughout my projects, abstracts, papers and PhD examinations, he was always eager to offer advice and help during our nearly weekly crosslinking experiments - all while managing to teach an engineer a few things about biology. The amount of passion and energy he has for research is inspiring. He is a role model for not just me, but everyone in the lab, and I hope to carry these same qualities onward in my career.

Dr. Brown - though he didn't have to - was always there, ready and willing to help with experiments and offering tips and suggestions for every situation. Throughout my 6 years here, I learned quite a bit about Montana, birding, and photography (perhaps too much). I truly appreciate and will miss your trove of knowledge and advice.

Our postdoc Dr. Samantha Bradford was a constant support for me for the entirety of my PhD journey - from sending me papers and resources before I had even joined the lab, helping me with every project and question, to even offering tips on shaping this dissertation. Working alongside her on every experiment was an incredible learning experience and I have deep admiration for her resilience and work ethic. I wish her the very best in her future endeavors.

A special thanks to Yilu Xie - our lab's unofficial mom - whose support extended beyond labwork. From advice (both in staining or life in general) to always checking in on my well-being even when she didn't have the time, her kindness never went unnoticed. I will miss our chats and daily coffee runs.

Though they weren't here for long, I would also like to acknowledge and appreciate Dr. Jungsub Kim, Dr. Shangbang Luo, Emily Farrah, Ceci Zhang, Dr. Satish Baggam, Dr. Jiyea Kim, and Shari Atilano for being extraordinarily helpful and supportive for the duration of my degree.

To my parents - thank you for being my backbone throughout this decade-long schooling. Without your love, support, and infinite patience this dissertation would not have been possible. I have no doubt you're just as (if not more) relieved than I am that it's finally finished.

Portions of the text of Chapter 1 of this dissertation are a reprint of the material as it appears in Bradford, S., Mikula, E., Xie, Y., Juhasz, T., Brown, D. J., & Jester, J. V. (2020). Enhanced Transepithelial Riboflavin Delivery Using Femtosecond Laser-Machined Epithelial Microchannels. *Translational Vision Science & Technology, 9*(6), Article 1. https://doi.org/10.1167/tvst.9.6.1, used with permission from TVST.

Portions of the text of Chapter 2 of this dissertation are a reprint of the material as it appears in Bradford, S., Joshi, R. P., Luo, S., Farrah, E., Xie, Y., Brown, D. J., Juhász, T., & Jester, J. V. (2024). In Vivo Femtosecond Laser-Machined Transepithelial

Nonlinear Optical Corneal Crosslinking Compared to Ultraviolet Corneal Crosslinking. *Translational Vision Science & Technology, 13*(10), Article 9. https://doi.org/10.1167/tvst.13.10.9, used with permission from TVST.

The text of Chapter 3 of this dissertation is a reprint of the material as it appears in Joshi, R., Bradford, S., Luo, S., Farrah, E., Xie, Y., Brown, D. J., Juhász, T., & Jester, J. V. (2025, March 3). Enhanced Riboflavin Stromal Delivery Using Microchannel-Assisted Iontophoresis for Corneal Crosslinking. *Translational Vision Science & Technology, 14*(3), Article 18. https://doi.org/10.1167/tvst.14.3.18 used with permission from TVST.

I would also like to acknowledge the following grants: NIH EY024600, NIH EY034070, and Research to Prevent Blindness, Inc. (RPB 203478). This study was made possible in part through access to the Optical Biology Core Facility of the Developmental Biology Center, a shared resource supported by the Cancer Center Support Grant (CA-62203) and Center for Complex Biological Systems Support Grant (GM-076516) at the University of California – Irvine, Irvine, CA.

ABSTRACT OF THE DISSERTATION

Applications of Laser Therapy for Anterior Cornea Drug Delivery and Treatment

By

Rohan Joshi

Doctor of Philosophy in Biomedical Engineering

University of California, Irvine, 2025

Professor James V. Jester, Chair

Keratoconus (KC) and post-Lasik ectasia, in addition to other ectatic disorders of the cornea are debilitating conditions characterized by the mechanical thinning and weakening of the corneal stroma. This leads to a distorted bulge in the cornea and results in heightened sensitivity to light and glare as well as a sharp decline in visual acuity. Glasses, contact lenses, and intrastromal implants (Intacs) can be used temporarily to correct vision but in more advanced stages of this condition, a corneal transplant is often required.

A recent method called corneal collagen crosslinking (CXL) is being tested to halt or reverse the progression of Keratoconus. This method involves soaking the cornea in a photosensitizer, Riboflavin (Rf) and undergoing ultraviolet-A (UVA) irradiation. This process causes the Rf to generate oxygen free radicals, causing covalent bonds to form between the corneal collagen fibers, which results in mechanical flattening and stiffening of the tissue. However, UVA light is cytotoxic and harmful to living tissue so specific parameters for CXL are used to minimize the exposure damage to the eye. These parameters limit the CXL to the anterior cornea and do not allow for control over

the treated area. Furthermore, UVA CXL requires complete epithelial debridement as the epithelial barrier prevents Rf molecules from penetrating into the stroma. This causes patient pain, an increase in recovery time, and a risk of infection.

Transepithelial CXL (TE CXL) is a new and active area of research with many different methods being tested in both clinical and laboratory settings. These commonly involve the use of chemical excipients such as Benzalkonium Chloride (BAK), ethylenediaminetetraacetic acid (EDTA), glutathione, and various vitamins to loosen the epithelial tight junctions. Regardless of method, TE CXL has yet to be able to reproduce the results of traditional UVA CXL, likely due in part to the reduced Rf penetration into the stroma or due to the nature of the single photon reaction that takes place at the surface epithelium.

To address these issues, we hypothesized several solutions to greatly increase the safety, efficacy, and time requirement for the CXL procedure. These include femtosecond (FS) laser-based micromachining of channels through the corneal epithelium and optimizing Rf osmolarity to increase Rf penetration into the corneal stroma, using our NLO CXL technology which can produce CXL at any depth and pattern without causing damage, and using iontophoresis to further increase Rf stromal penetration while also drastically reducing treatment time.

This body of work details modifications and improvements to both traditional UVA CXL and TE CXL with focus on improving safety, efficacy, and treatment time. It also presents the results of laser application on studies focusing on root causes or treatment of other ocular conditions such as Keratoconus and Meibomian Gland Dysfunction (MGD

Introduction

Keratoconus

The corneal stroma is primarily composed of a collagen matrix which provides both structural strength and the necessary curvature to properly refract light onto the retina. An alteration in the mechanical integrity of this matrix affects the eye's overall refractive power. Keratoconus and post-LASIK ectasia are two corneal ectatic disorders that cause the collagen structure to become biomechanically compromised, leading the cornea to undergo thinning, develop a conical protrusion, and astigmatism.

Keratoconus is a non-inflammatory disorder characterized by the gradual weakening of corneal biomechanics and affects 1 in 2,000 individuals in the general population and is the leading cause for corneal transplantation. Post-LASIK ectasia is a closely related condition that arises as a rare complication of refractive surgery with an estimated incidence of 1 in 4,500 patients.

Motivation

A promising novel therapeutic method - originally introduced by Spoerl and Wollensak and recently approved by the FDA - involves mechanically reinforcing the weakened stromal tissue by inducing CXL through ultraviolet-A (UVA) irradiation. UVA CXL has shown success in slowing or halting disease progression in KC patients and may delay or even prevent the need for future surgery.

However, UVA CXL lacks precision over the region of crosslinking and exposes more tissue to the harmful UVA irradiation and free radical damage than necessary. In

addition, the procedure is both lengthy (30 minutes) and painful for the patient as complete epithelial debridement is required. This dissertation explores modifications and improvements to both traditional UVA and TE CXL with the addition of FS-machined microchannels (MC), nonlinear optical (NLO) CXL, optimized Rf osmolarity, and iontophoresis.

Crosslinking

The standard protocol for UVA CXL (also known as the Dresden Protocol) requires removal of the corneal epithelium to allow stromal saturation with a photosensitizing agent (0.1% Rf in PBS containing 20% high fraction dextran). This Rf solution is topically applied every 2 minutes for 30 minutes to ensure stromal penetration. The cornea is then exposed to UVA light at a 370 nm wavelength with an irradiance of 3 mW/cm^2 - delivering a total energy dose of 5.4 J/cm^2 over 30 minutes. The UV exposure photoactivates the Rf, leading to the generation of reactive oxidative species (ROS) and induces CXL between and within the collagen fibrils. This CXL enhances collagen-associated autofluorescence (CAF) which can be seen by exciting at 760 nm and detecting emission in the 400-450 nm range is shown in Fig 1.

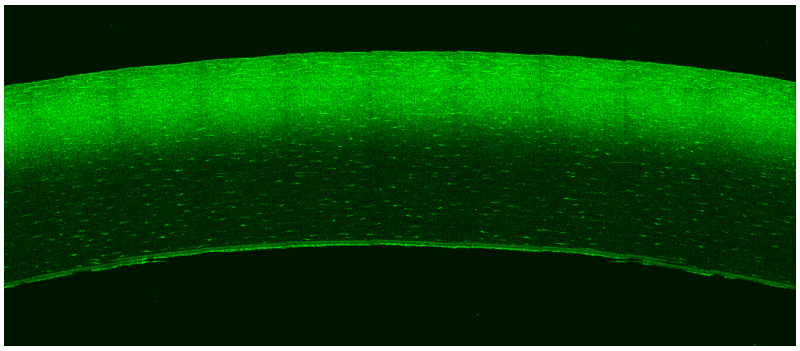

Figure 1: Enhanced CXL Post-UVA CXL
Enhanced CAF between 400-450 nm in a UVA CXL treated cornea (Dresden Protocol)

UVA CXL has been shown to increase corneal stiffness by up to 300%, along with a threefold increase in the corneal elastic modulus. This treatment has shown a delay in the progression of ectatic corneal disease and improved visual acuity. Clinical studies have further shown that CXL results in corneal flattening of approximately one diopter within 6 months persisting for at least 24 months. This suggests a broader application of this method for the treatment of low refractive errors.

This method has been shown to induce several structural and cellular changes in corneal tissue, including dose-dependent cytotoxicity, stromal haze, and up to a 12% increase in collagen fibril thickness in the treated region. Keratocytes and endothelial cells are both susceptible to apoptosis in the crosslinked volume. Despite keratocyte repopulation beginning one month post-treatment in animal models, the timeline for full recovery is inconsistent. Wollensak reported complete keratocyte activity by 6 weeks but other studies show persistent acellular regions and apoptotic changes near the irradiation region. Though keratocyte death is considered manageable, damage to the endothelial cells is of greater concern due to their non-regenerative nature and importance in maintaining corneal deturgescence. UVA irradiance over 0.36 mw/cm^2

has been shown to cause irreversible damage and so the parameters of the Dresden Protocol were optimized to minimize this risk. One limitation requires a minimum corneal thickness of 400 μm as a safe threshold. Unfortunately, this means patients with advanced Keratoconus are ineligible for treatment and shows a clear limitation on current clinical practice.

Another key limitation of UVA CXL is its lack of precision as it relies on single-photon excitation, leading to superficial treatment penetration. A single UVA photon excites Rf to a singlet excited state. If intersystem crossing to the triplet state is achieved, an oxygen free radical is produced which can initiate CXL. Otherwise, the Rf returns to the ground state through green fluorescence emission. As the UVA photons only excite Rf along the optical path, crosslinking primarily occurs within the anterior 300 μm of the stroma and has a diminishing effect at greater stromal depths due to UVA light being quickly attenuated by depth, resulting in reduced treatment efficiency in the posterior of the stroma for patients with advanced thinning. Prolonged excitation results in photobleaching of the Rf, further reducing chances for effective CXL. Furthermore, oxygen - essential in ROS generation - rapidly depletes during treatment. Studies show that oxygen levels fall within 15 seconds of UVA CXL and are exacerbated by an accelerated CXL protocol - severely limiting efficacy. A transepithelial approach preserves the epithelium minimizes patient pain and discomfort but still results in epithelial damage and reduced Rf diffusion, leading to suboptimal CXL.

CXL advancements need to mitigate these drawbacks by focusing on a precise control over the region of crosslinking while reducing exposure of healthy tissue to UVA light. Ideally, the treatment should allow treatment of specific stromal regions, allow a

precise depth-selective activation of CXL, apply to patients with thin corneas, and minimize cellular damage. This can be achieved by finding a method to increase the stromal Rf saturation to generate more crosslinks, using the controllable NLO CXL to generate crosslinks in the posterior stroma, modifying the osmolarity of the Rf solution to temporarily swell the eye to the required 400 μm, and reducing the treatment time from 30 minutes.

Chapter 1: Epithelial Microchannels

Introduction

Various TE methods have been developed to address the need for a less invasive but still effective method for Rf stromal delivery. Many of these use chemical enhancers such as BAK, EDTA, glutathione, and various other vitamins. [1-2] Though these partially improve Rf diffusion, TE remains inferior to the standard epi-off method as it is unable to achieve sufficient stromal saturation for effective CXL. [3-4] Additionally, some of these excipients - such as BAK - are cytotoxic and result in damage to the epithelial cells, lowering this method's safety in a clinical setting. [5-15]

Previous research from our laboratory has focused on different ways to improve the CXL procedure. Bradford et al. (2017) developed nonlinear optical (NLO) crosslinking - a femtosecond (FS) laser-based technique that induces localized and depth-selective CXL using two-photon Rf excitation. [5] This method enables precision to the micron scale and avoids the broad surface exposure that occurs in standard UVA CXL. [16-32] In 2020, Bradford et al. developed FS-machined microchannels which significantly enhanced TE Rf delivery into the stroma, avoiding the need for epithelial debridement while also improving the safety of the procedure. Not only did this technique produce stromal Rf concentrations comparable to the standard epi-off UVA CXL, it also minimized stromal and epithelial cell damage relative to the use of chemical enhancers such as BAK, typically used in TE CXL [22, 33, 34]. **Though I did not directly contribute to these prior studies, I will discuss the methodologies and**

protocols as they were an important foundation for the study in this and future chapters.

In this study, we investigate a novel method for enhancing transepithelial Rf delivery using FS laser-based micromachining to create epithelial microchannels to facilitate the diffusion of Rf into the stroma without epithelial debridement or use of chemical enhancers. In addition, we evaluated the combined result of this method with NLO CXL to assess Rf penetration and cellular damage with TE BAK-assisted Rf delivery.

Methods

64 ex vivo rabbit eyes were obtained from a supplier (Pel-Freez, Rogers, AR) and shipped overnight on ice. On arrival, eyes were rinsed in phenol-free, low glucose DMEM (Sigma Aldrich, St. Louis, MO) [35]. Epithelial integrity was checked using Lissamine green (10 mg/ml in PBS) staining. Defective eyes were excluded from treatment or used as epi-off controls.

Prior to treatment, all eyes were incubated for 2 hours at 37°C in a humidified incubator with 5% CO_2. Rf was administered using one of three methods:

1. FS-machined microchannels (G1)
2. Transepithelial with BAK (G2)
3. Dresden Protocol with complete epithelial debridement (G3)

Each eye was assigned to a treatment group based on solution and Rf delivery method with subgroups variations on application (20% dextran or 1% methylcellulose) and Rf

concentrations (0.1%, 0.5%, or 1.0%). In G1, a Tooke knife was used to debride the epithelium over an 8 mm central region of the cornea. Rf drops (0.1%, 0.5%, or 1.0%) were dissolved in 20% dextran and were applied every 2 minutes for 30 minutes. In G2, the Rf solution with 0.01% BAK and 1% methylcellulose was applied every 2 minutes for 30 minutes. In G3, eyes received microchannels and were then treated with 1% Rf in 1% methylcellulose every 2 minutes for 30 minutes.

Femtosecond Laser-Based Epithelial Micromachining

FS micromachining was performed with a 1030 nm, 1 kHz amplified laser (OneFive Origami, NKT Photonics, Denmark) with a custom NLO CXL delivery method as shown in Fig 2.

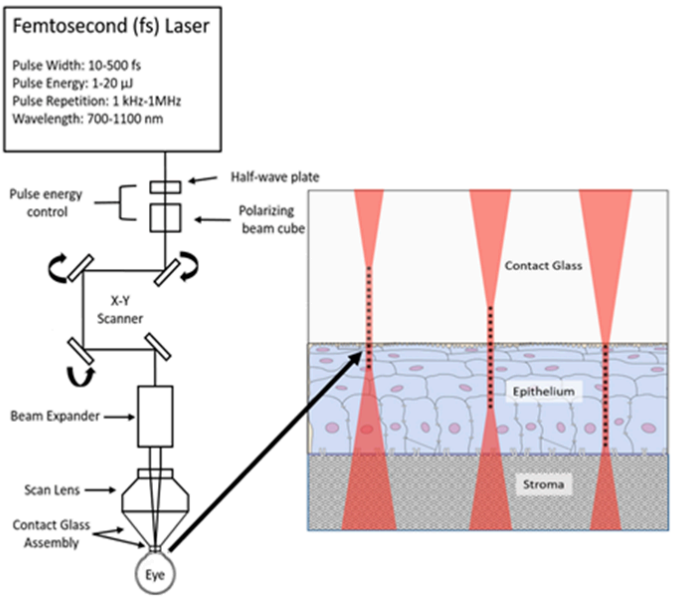

Figure 2: Epithelial Micromachining

Microchannels were generated by directing the 1030 1 kHz, amplified laser beam with a pulse energy of 5 or 10 µJ, 50 µm spacing, and depth of 25 µm.

Pulse energy was adjusted to 5 or 10 μJ using a half-wave plate and polarizing beam splitter. Depth alignment and laser focus was verified before the procedure by machining holes into a silicone sheet (Fig 3) to make sure channels were generated only in the surface epithelium and not the underlying stroma. These channels were generated in a grid pattern (raster scan) in the central 6 mm of the cornea with either a 50 or 100 μm spot spacing (400 or 100 channels/mm^2). The scanning mirrors and microchannel patterns were controlled with our custom Labview software.

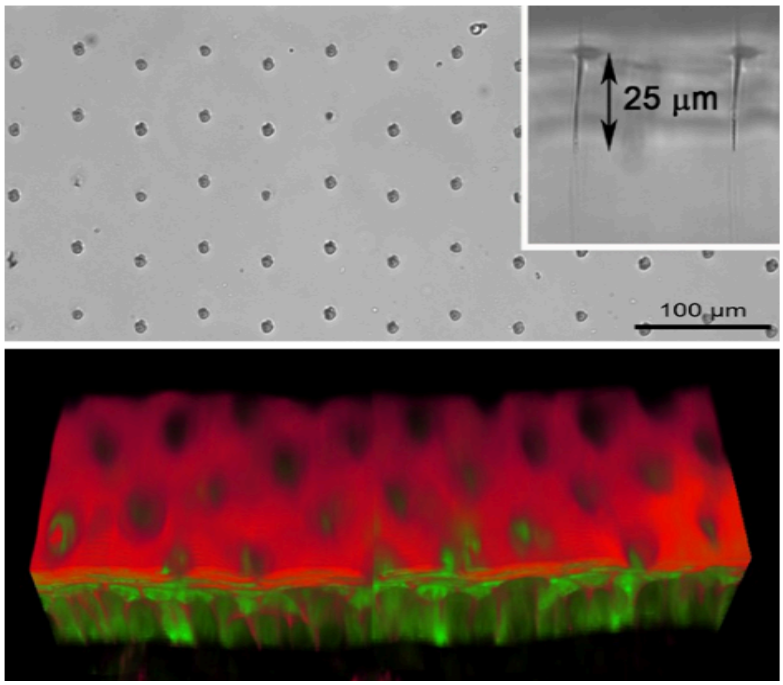

Fig 3: Channel Spacing in Silicone and Epithelium

A grid of microchannels with 50-μm spacing and 25-μm depth was cut into a silicone sheet for demonstration of the pattern (top). A three-dimensional reconstruction of a corneal section stained with phalloidin and propidium iodide shows the same grid placed on the surface of the corneal epithelium.

NLO CXL

A separate set of eyes underwent NLO CXL (Fig 4) with the 760 nm FS amplified laser pulses through the same (above) delivery method used for generation of microchannels. These eyes were cultured a) for 3 hours or b) overnight. All corneas were then fixed in 2% paraformaldehyde (PFA) and stained with phalloidin (1:100) and propidium iodide (0.01 mg/ml) to view the actin filaments and assess cell death.

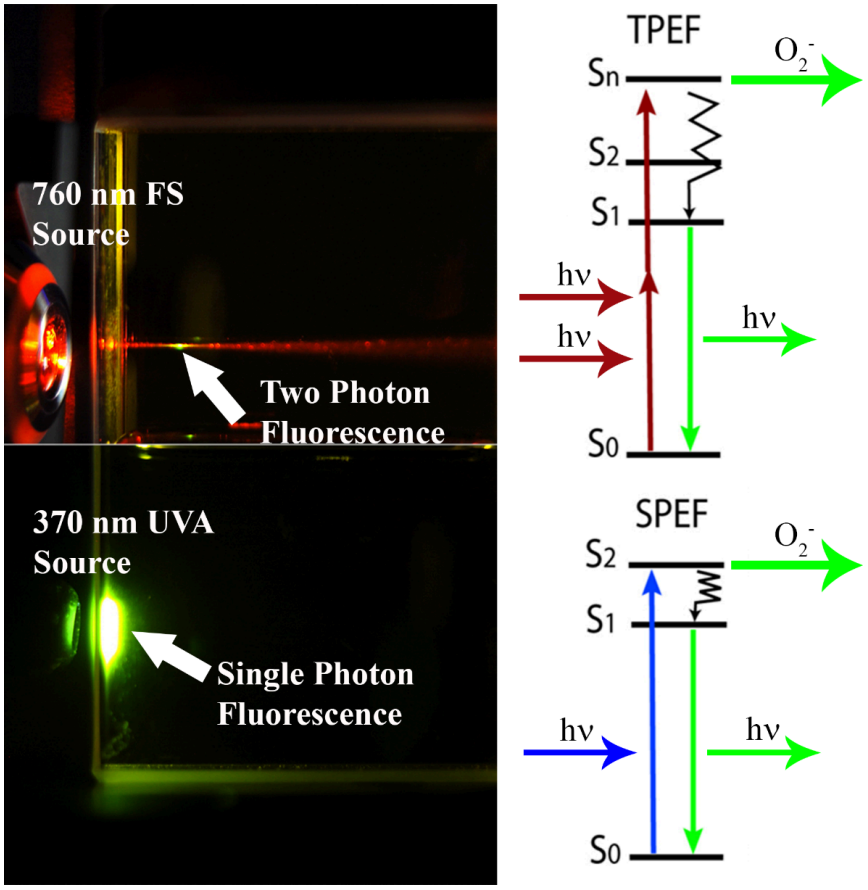

Figure 4: One vs Two-Photon Excitation

A) Two photon excitation of Rf solution using a 760 nm FS laser with corresponding Jablonski diagram demonstrating two photon excitation.
B) Single photon excitation using a 370 nm light source with corresponding Jablonski diagram.

Quantifying Stromal Rf Concentration

First, excess surface Rf was removed using cotton gauze. The entire cornea was then excised around the limbus and a 8 mm central button was cut out using a trephine. These buttons were placed in 1 ml of PBS and stored overnight to allow the Rf to elute from the buttons.

A SpectraMax Gemini XPS plate reader (Molecular Devices, Sunnyvale, CA) was used to quantify the fluorescent intensity of the eluate with excitation at 380 nm and emission at 540 nm. A standard curve of stromal Rf concentrations was generated using serial dilutions of the stock Rf solution. Using linear regression (R^2 values), fluorescence intensity was converted to Rf concentration (µg/ml) values.

Results

Rf Stromal Concentration

Figure 5 shows a comparison of Rf concentrations for the different treatment groups. In the Dresden Protocol control group (epi-off), mean stromal Rf concentrations with 0.1%, 0.5%, and 1.0% Rf were 9.2 ± 1.9, 37.0 ± 6.9, and 66.6 ± 7.1 µg/ml respectively. The transepithelial group using BAK had significantly lower Rf concentrations at 3.2 ± 0.7, 9.3 ± 1.8, and 19.2 ± 5.0 µg/ml respectively - only 25-35% of the control group. FS micromachining with 5 µJ pulses and 50 µm spacing yielded an average stromal Rf concentration of 34.4 ± 3.0 µg/ml - nearly two fold higher than the BAK group and 50% of the epi-off control. This value was comparable with that obtained from complete epithelial debridement and 0.5% Rf which we previously reported for

NLO CXL with amplified pulses. Interestingly, increasing the microchannel spacing to 100 µm (100 channels/mm^2) resulted in a 50% reduction in Rf concentration [36-39], comparable to that achieved by the BAK group. An increase in pulse energy from 5 to 10 µJ also halved the concentration - possibly due to a reduced Rf diffusion from epithelial damage.

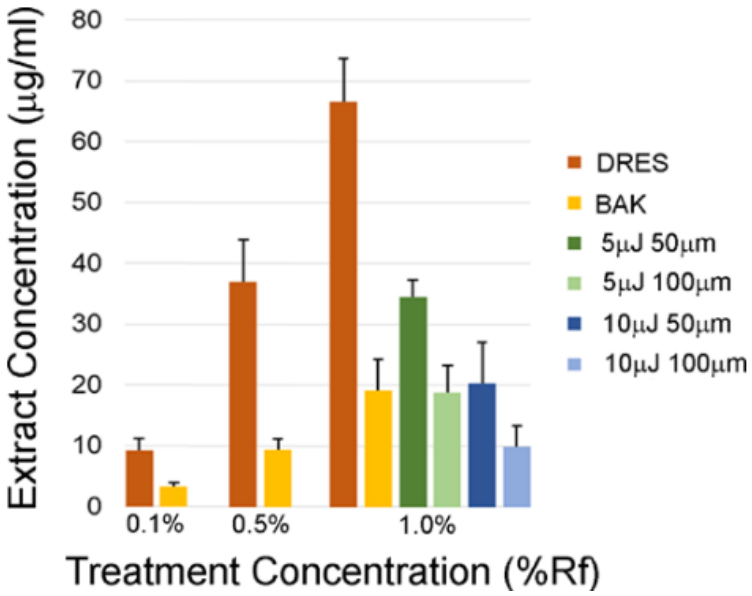

Fig 5: Stromal Rf Concentration

Stromal Rf concentration within the transepithelial groups was highest using 5-µJ, 50-µm spaced channels, 34.4 ± 3.0 µg/mL. This was not significantly different from DRES using 0.5% Rf required for NLO CXL. Channels created with 10-µJ pulse energy but allowed a significantly lower concentration of Rf to diffuse into the stroma.

Post-treatment Staining

Figure 6 shows cellular staining of the corneas. Samples were organ cultured for 24 hours and stained to determine epithelial and keratocyte integrity following transepithelial NLO CXL using either BAK + 0.5% Rf or microchannels. Figure 6A,

showing a cornea treated with BAK + 0.5% Rf followed by NLO CXL, showed extensive damage to the epithelium and keratocytes in addition to an acellular zone extending beyond the crosslinked area (double headed arrows). The epithelium was severely damaged and only loosely attached following the 24 hours of culture. Cytotoxicity from the BAK is indicated by stromal keratocyte death (asterisks) outside of the treatment region. Figure 6B shows a cornea treated with microchannels without the addition of BAK and followed by 3 hours of culture. There was no noticeable epithelial damage or keratocyte death. Arrows show the locations of the drilled microchannels which can still be seen due to the intact epithelium. Finally, figure 6C shows a cornea that received NLO CXL followed by microchannels. Here, the region of keratocyte death corresponded to the targeted region of crosslinking with the surrounding epithelial and stromal cells remaining undamaged.

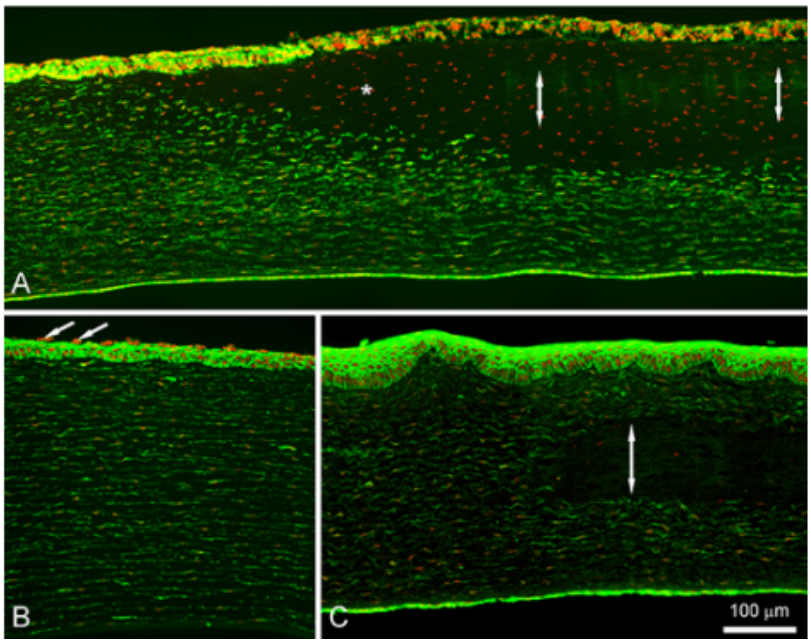

Fig 6: Cellular Staining Post-BAK and MC Rf Administration

(A) Cross section of a cornea treated with 0.5% Rf eye drops containing

0.01% BAK, followed by transepithelial NLO CXL. The cornea was rinsed and cultured for 24 hours and then stained with phalloidin (green; 1:100) and propidium iodide (red; 0.01 mg/mL). (B, C) Cross sections of corneas treated with 5-μJ pulse energy microchannel Rf delivery alone (B) and followed by NLO CXL (C), cultured for 3 hours (B) or 24 hours (C), and stained with phalloidin and propidium iodide. Regions of CXL and examples of visible microchannels are marked with arrows, and cellular death outside this region is marked with an asterisk (A).

Discussion

No method of transepithelial CXL has yet been able to match the efficacy of standard UVA CXL. Despite various approaches, treatments remain less effective and frequently damage the epithelium. This limits their ability to reduce post-op recovery time, risk of infection, and patient pain. This is primarily due to the corneal epithelium, which poses a barrier to both the diffusion of Rf as well as the penetration of UV.

Due to its precise and controllable nature, NLO is a promising alternative by enabling crosslinking at specific stromal depth while minimizing damage to the anterior and posterior cornea. Additionally, provided a sufficient stromal Rf saturation, the epithelium will remain undamaged. This opens the possibility of personalized topography-guided CXL.

This study demonstrates that FS generated epithelial microchannels can significantly enhance Rf delivery. Stromal concentrations were approximately 50% of those obtained through complete epithelial removal and twice those obtained with BAK-enhanced transepithelial delivery. More importantly, this was done with minimal damage to the epithelium and stromal cells as compared to BAK use. Furthermore, BAK's cytotoxicity resulted in extensive cellular damage outside of the crosslinked

region and lowered the efficacy of NLO CXL by defocusing the laser beam at the epithelium and lowering the efficiency of two photon excitation.

A higher pulse energy (10 μJ) interestingly resulted in lower stromal Rf concentrations compared to the lower 5 μJ treatment. The expectation was that larger holes would enable more Rf diffusion into the stroma. A possible reason for this could be that the higher energy use may have resulted in greater damage to the epithelium and impeded Rf diffusion. Further studies are needed to investigate and optimize pulse energy, channel separation, and channel patterns.

Another limitation is the Rf extraction method used. 8 mm corneal buttons were taken but only the central 6 mm received microchannel treatment, which may have resulted in lower Rf levels in the microchannel eyes as compared to the BAK and control groups which received treatment in the full 8 mm region. This suggests that microchannel efficacy is possibly even greater than what was reported. In future studies we will explore whether lowering Rf concentrations or modifying the microchannel variables will provide better results.

Chapter 2: Microchannels: UVA vs NLO

Note on Prior Publication

Portions of this chapter (Methods and Results) have been previously published as:

Bradford, S., Joshi, R. P., Luo, S., Farrah, E., Xie, Y., Brown, D. J., Juhasz, T., & Jester, J. V. (2024). In vivo femtosecond laser machined transepithelial nonlinear optical corneal crosslinking compared to ultraviolet corneal crosslinking. *Translational Vision Science & Technology*, 13(10), 9. https://doi.org/10.1167/tvst.13.10.9

I contributed to this manuscript as a second author with responsibilities including cellular staining and imaging, creating some of the published figures and tables, and assisting with crosslinking experiments.

Introduction

Transepithelial CXL techniques have not been able to match the efficacy of epithelium-off approaches in the clinical setting. Kmax stabilization has only been observed in approximately 43% of patients that underwent epi-on CXL as compared to the 93% that received the standard epi-off (Dresden Protocol) CXL. [39-43] An important marker of crosslinking - the stromal demarcation line - was also shallower in epi-on procedures showing reduced efficacy. Furthermore, similar to epi-off CXL, epi-on methods still result in epithelial injury and postoperative pain for the patient. [43-48] BAK, a commonly used chemical enhancer in epi-on Rf delivery loosens the epithelial tight junctions and causes cellular damage due to its cytotoxic effects. [44, 49] Taneri et al. also note patient reports of discomfort due to frequent epithelial defects which are only exacerbated by an accelerated epi-on protocol. [47] This suggests that damage to the epithelium results from two causes: a) the Rf delivery method and b) epithelial exposure to UVA. In order to deem transepithelial CXL both safe and effective, not only is maximum Rf stromal penetration required, but the epithelium must also be protected from phototoxicity.

We have previously shown that microchannels generated by FS epithelial micromachining significantly enhance stromal Rf delivery and result in 50% Rf concentration as that achieved by complete epithelial removal. [46] Additionally, we have developed a method for nonlinear crosslinking using 1 kHz FS laser pulses in which precise control of crosslinking is possible within the focal volume of the laser - all while operating at a power level below the American National Standards Institute (ANSI)

threshold of 46.1 mW. [50] Furthermore, the treatment zone can be targeted within the anterior stroma to allow the maximum crosslinking effect to take place without damaging the surrounding tissue.

We hypothesize that a combination of microchannel-assisted Rf delivery and the precision of NLO CXL would allow for a much safer and effective transepithelial CXL without the common risks associated with UVA CXL. In this project, we compared the safety and efficacy of the combined microchannel-assisted NLO CXL with microchannel-assisted UVA CXL.

Methods

Riboflavin Delivery Optimization

Tissue Preparation

Intact rabbit eyes were shipped (Pel-Freez, Rogers, AR, USA) as previously reported. [5-6, 46] Briefly, eyes were rinsed in Dulbecco's modified Eagle's medium (Sigma Aldrich, St. Louis, MO, USA), inspected for epithelial damage using Lissamine green staining (10 mg/mL in phosphate-buffered saline [PBS]; Sigma Aldrich), and incubated prior to treatment. Eyes showing epithelial staining, indicating damage, were discarded or used as control corneas treated by epithelial debridement. After incubation, eyes were imbibed with Rf solution using one of two techniques: epithelial debridement followed by 30 minutes of dripping with Rf solution in 20% high fraction dextran or epithelial micromachining followed by 30 minutes dripping of Rf solution of varying

osmolarities between 200 and 400 mOsm (osmolarities were varied by varying the concentration of NaCl in the solution). Methylcellulose solution was used in place of dextran with MC treatment because it is iso-osmotic and better suited for use with intact corneal epithelium than dextran that can dehydrate the cornea.

The creation of MCs was achieved using our previously reported protocol. [5] Briefly, a 1030-nm, 1-kHz, amplified FS laser beam (One Five Origami, NKT Photonics, Birkerod, Denmark) was directed into previously described delivery optics. [46] Pulse energy was adjusted to 5 μJ, and the maximum MC depth was set to 25 microns to ensure that the MCs did not extend into the corneal stroma. The pattern chosen for this experiment was 50-μm spaced MCs within a 6-mm diameter circular region, equivalent to 400 MCs/mm^2. This pattern was chosen because it had previously been shown to produce sufficient levels of stromal Rf without detectable epithelial damage. [5]

Measuring Stromal Riboflavin Concentration

Measurements of stromal Rf concentration were done as previously described. [5] After Rf treatment, the epithelium was removed, followed by removal of the entire cornea from the globe around the limbus, and a central corneal button was cut using a 6-mm trephine. The button was then placed in 1 mL PBS solution and left to soak overnight. Care was taken to make sure that the corneal button was removed and placed in fluid within 4 minutes or less to avoid loss of Rf into the anterior chamber.

The concentration of Rf in the eluate, in mg/mL, was then measured using a Spectramax Gemini XPS fluorescence plate reader (Molecular Devices, Sunnyvale, CA, USA) with 380 nm excitation and 540 nm emission as previously published. [5] Serial

dilutions of the stock Rf solution were used to create a standard curve, which was then used to convert the measured intensity values of each into a measure of μg/mL. Standard curve calculations were performed each time the experiment was repeated to avoid any day-to-day errors.

Optimizing Rf Photoactivation

Since UVA single-photon photoactivation of Rf using TE Rf delivery requires UVA light to pass through the corneal epithelium before photoactivation of stromal Rf, we assessed the ability of the standard UVA CXL procedure to achieve stromal CXL through this layer, as well as the layer of Rf remaining on the surface of the epithelium. Specifically, we tested the hypothesis that UVA focused through the Rf-treated corneal epithelium would lead to absorption of UVA light and reduce stromal CXL compared to NLO CXL, which focuses infrared 1030-nm FS light through the epithelium that is not absorbed by Rf.

Since the standard UVA CXL approach continues to apply dextran-containing Rf solution to the cornea during UVA irradiation, a layer of solution remains on the surface of the epithelium, potentially adding to the shielding effect of the Rf already contained within the epithelium itself. To assess the shielding effect of this layer, UVA transmittance alone was first measured through different thicknesses of Rf solution between 30 and 210 μm. This was accomplished by measuring the power of a UVA light transmitted through Rf solution trapped between two glass coverslips separated by gaskets of varying thickness.

To test the effects of shielding on crosslinking, ex vivo rabbit eyes were treated with epithelial MCs followed by 30-minute application of 1% Rf in 1% methylcellulose in

PBS. Eyes were then treated with UVA CXL for 30 minutes, with continued application of 1% Rf in 1% methylcellulose solution or rinsed with PBS and treated with 1% Rf in PBS alone.

After treatment, corneas were removed and fixed overnight in 2% paraformaldehyde (PFA; Mallinckrodit Baker, Phillipsburg, NJ, USA), then sectioned and imaged for CXL-induced collagen autofluorescence (CAF), as previously reported. Briefly, corneas were cut into 200-µm-thick sections using a vibratome (Campden Instruments, Loughborough, UK) and irradiated with a 760-nm FS laser light, collecting the 400- to 450-nm emission spectra within the CXL regions of corneal sections using either a Leica SP8 (Beckman Laser Institute; Leica, Wetzlar, Germany) or Leica Stellaris 8 multiphoton confocal microscope (Leica) and Chameleon FS laser (Coherent, Santa Clara, CA, USA).

Live Rabbit Model

A comparison of MC NLO CXL and MC UVA CXL was performed in the right eyes in a total of 36 live New Zealand albino rabbits under 6 months of age. All animals were treated according to the Association for Research in Vision and Ophthalmology statement on the use of animals in vision research, and experiments were approved by the Institutional Animal Care and Use Committee (IACUC) of the University of California, Irvine (AUP 23-016). Eyes were followed sequentially and rabbits sacrificed at 2 weeks, 1 month, or 2 months (n = 3 male and 3 female/time point). Rabbits were followed postsurgery to monitor in vivo wound healing via Lissamine green staining, optical coherence tomography (OCT) imaging, and Cochet–Bonnet aesthesiometry. After sacrifice, corneas were removed and examined for CAF to verify the presence of

CXL, followed by immunohistochemistry (IHC) to analyze the cellular wound-healing response.

Preoperative Evaluation

Baseline esthesiometry measurements were taken on both eyes of each rabbit using a Luneau Cochet–Bonnet Aesthesiometer (Western Ophthalmics, Lynnwood, WA, USA) on unanesthetized rabbits as described below. Rabbits were then sedated with a subcutaneous injection of 30 to 50 mg/kg ketamine hydrochloride and 5 to 10 mg/kg xylazine (MWI Animal Health, Boise, ID, USA), and OCT images were taken of each eye using a Topcon DRI OCT Triton Plus (Topcon, Tokyo, Japan) for baseline measurements of epithelial and stromal thickness and corneal haze as described below.

Surgery: MC Formation

The creation of MCs was achieved as described above according to our previously reported protocol. [5] Corneas were then imbibed with 1% Rf solution in 1% methylcellulose for 30 minutes.

UVA CXL

UVA CXL was performed using the protocol previously described. [46] Rabbits were sedated as described above followed by topical anesthesia using 0.5% tetracaine hydrochloride (Alcon, Ft. Worth, TX, USA) to prevent pain during treatment. The central 8 mm of the cornea was exposed to 3 mW/cm$_2$ 370 nm UVA light for 30 minutes with continued application of 1% Rf in PBS every 5 minutes. After treatment, the rabbits received a subcutaneous 0.1-mL injection of buprenorphine hydrochloride (Reckitt Benckiser Healthcare Ltd., Slough, UK) and 0.3% gentamycin sulfate eye drops

(Allergan, Inc., Irvine, CA, USA) in the treated eye. Gentamycin drops were repeated three times daily for 3 days to prevent infection.

NLO CXL

After Rf imbibition as described for UVA CXL, amplified NLO CXL was performed in the same manner as previously published. [45] Sedated animals received a drop of topical ophthalmic 0.5% tetracaine hydrochloride (Alcon). The central 4 mm of the right corneas then underwent amplified NLO CXL using 760 nm FS light, 2 μm line separation, 0.3 μJ/pulse pulse energy, 30 mW total power, and scan speed of 20 mm/s. Rabbits received the same after treatment care as UVA CXL rabbits to prevent pain and infection.

In Vivo Measurements

Lissamine Green Staining

For 3 consecutive days after CXL, rabbits in all groups were monitored for epithelial damage via Lissamine green staining (10 mg/mL in PBS; Sigma Aldrich). After sedation, the treated cornea of each rabbit received a drop of Lissamine green solution to stain any epithelial defects. The cornea was then rinsed with PBS and images taken using a Celestron Handheld Digital Microscope Pro (Celestron, Torrance, CA, USA). Images were imported into QuPath open-source software for analysis of epithelial wound dimensions. The area that had taken up the stain was measured at 24, 48, and 72 hours, through to full epithelial healing.

OCT

OCT imaging was also performed on both eyes of anesthetized rabbits (three per treatment group) before surgery and at each time point after surgery using a Topcon

DRI OCT Triton Plus (Topcon) system. These images were used to measure epithelial and stromal thickness, as well as the depth of demarcation line throughout healing.

Cochet–Bonnet

Cochet–Bonnet aesthesiometry was performed on all rabbits prior to surgery and at each time point after surgery to measure the nerve damage in both treatments using a Luneau Cochet–Bonnet esthesiometer. For this, the central cornea of an awake rabbit was probed with the esthesiometer's fiber at the maximum length. If no response was observed, the length was shortened by half of a centimeter, thereby increasing the force, and the procedure repeated until a blink reflex was reached. This process was repeated four times, and the mean value was recorded for each rabbit at 7, 14, 21, and 28 days postoperatively.

Sacrifice and Tissue Preparation

Animals were sacrificed at 2 weeks, 1 month, or 2 months post treatment by an intravenous injection of Euthanasia III (Vedco, Inc., St. Joseph, MO, USA) into the marginal ear vein. Immediately after sacrifice, corneas were fixed in situ under 20 mm Hg pressure via perfusion of 2% PFA in PBS to maintain the in vivo collagen structure, as described in previous studies [46].

Corneas were then removed and allowed to fix overnight. Each cornea was cut through the center, perpendicular to NLO CXL scan lines when relevant. Half of the cornea was then vibratome sectioned and evaluated for CAF as discussed above. The remaining half was embedded in OCT and cryosectioned, and 10-μm-thick sections were prepared for IHC staining and imaging using DAPI (1:2000) and rhodamine phalloidin (1:100) to detect keratocytes and epithelial cells.

Tissue Imaging

Two-photon detection of corneal CAF was done as described above. [5-6, 35, 46, 50] Regions of CAF were used to confirm the presence of CXL within each sample. If the region of CXL could not be found in a sample, that sample was removed from all other portions of the study. Three samples from the 2-month NLO CXL group were removed from the study due to their lack of confirmed CXL.

Fluorescent imaging was also performed on the stained cryosections by using 488-nm excitation and collecting at 500 to 550 nm to observe cellular differences between the two groups using a Leica DMI600B (Leica) with Metaview Image capture. Analysis of these images was performed in QuPath imaging software to measure the depth of any acellular zones, reported as the percentage of the stromal depth of the section and the keratocyte densities within sections. To measure the cellular density, cell counting was performed within a 6-mm-wide rectangle within the 10-μm-thick sections and reported as cells/mm^3.

Statistical Analysis

Statistical analysis was performed using the Tukey–Kramer method for a multiple-comparison analysis of variance in statistical software (SigmaStat, San Jose, CA, USA). Groups were considered to have a statistically significant difference with a P value of less than 0.05.

Results

Riboflavin Delivery Optimization

Effects of Osmolarity

Though not significant, the highest calculated stromal Rf concentration was achieved with the 300-mOsm solution (Fig 7). These results indicate that the optimal osmolarity is likely equivalent to that of the natural tear film.

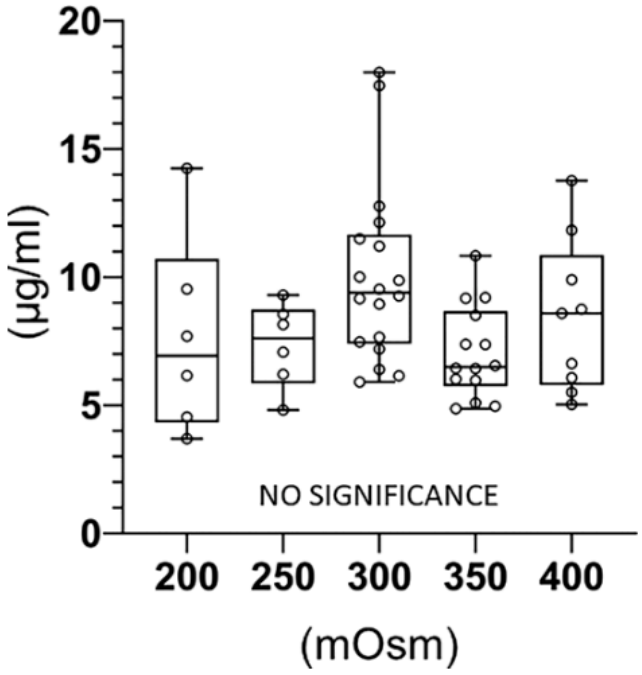

Figure 7: Riboflavin Osmolarity

Stromal Rf concentration values, reported in µg/mL, after being treated with MC machining and 30 minutes of dripping with Rf solution while varying osmolarity between 200 and 400 mOsm. No values are significantly different.

To test this hypothesis, we next performed MC UVA CXL on ex vivo rabbit eyes using a 30-minute UVA exposure as described above. Eyes that were continually treated with topical Rf in methylcellulose every 5 minutes during UVA exposure showed no CAF or stromal CXL (Fig 8B). However, eyes that were rinsed with 50 mL PBS to remove surface Rf prior to UVA exposure for 30 minutes and continued dripping with Rf in PBS showed strong CAF within the stroma (Fig 8C). Furthermore, when eyes were incubated overnight in organ culture and then removed, fixed, cryosectioned, and

stained for live/dead biomarkers, eyes treated with the standard Rf application showed no damage to either the epithelium or stroma (Fi. 8D). By contrast, eyes that were rinsed of Rf before UVA CXL and then organ cultured showed marked thinning and damage to the corneal epithelium in addition to loss of anterior stromal keratocytes (Fig 8E).

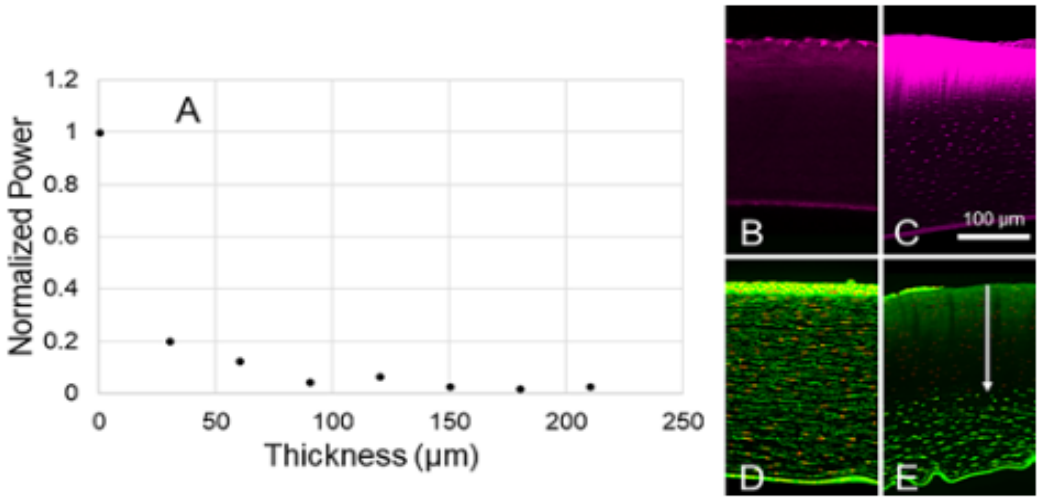

Figure 8: UVA Transmittance through Rf Barrier

(A) The dropoff in UVA power detectable through increasing thicknesses of Rf solution. (B, D) CAF and cellular damage detected after 24 hours in corneas after MC UVA CXL with continued Rf dripping. (C, E) Corneas were rinsed before UVA CXL began and did not receive continued dripping.

UVA CXL Versus NLO CXL

Epithelial Damage: Lissamine Green Staining, Cochet–Bonnet, and OCT

While rabbits receiving MC UVA CXL all showed epithelial defects after 24 hours, averaging 23.89 ± 5.6 mm^2 (Figs 9A, 3C), those treated with MC NLO CXL showed no epithelial damage (Fig 9B). Eyes showing epithelial defects also healed by day 3 after UVA CXL (Fig 9C).

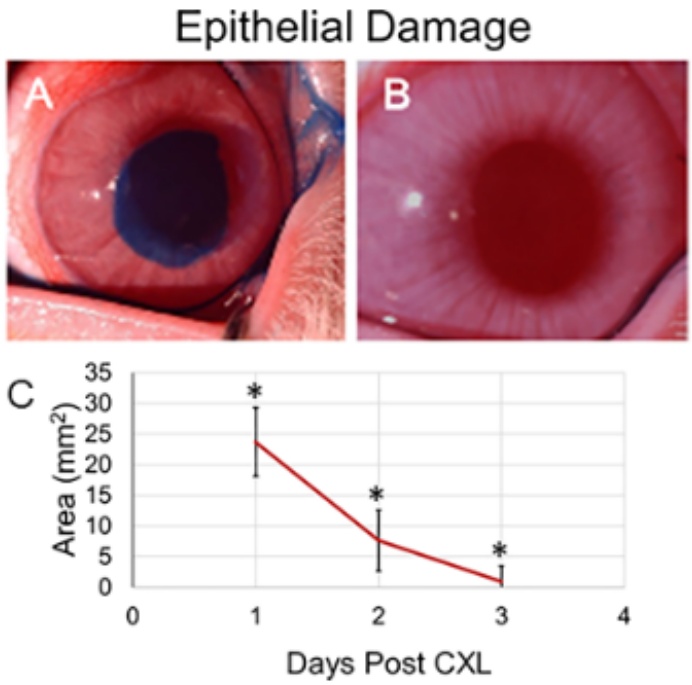

Figure 9: Lissamine Green Epithelial Staining

Corneas were stained with Lissamine green for 3 consecutive days following each CXL procedure. (A) A representative epithelial wound 24 hours after MC UVA CXL and (B) lack of wound 24 hours after MC NLO CXL. The graph shows the wound area measured each day in MC UVA CXL eyes, which fully heals by day 3. All days showed a significant decrease in wound area, indicated with asterisks.

Rabbits receiving MC UVA CXL also showed a complete loss of corneal sensitivity after 24 hours (Fig 10), averaging 0.83 ± 0.24 cm needed to elicit a blink reflex compared to the control value of 4.25 ± 0.35 cm. The sensitivity of the UVA CXL–treated eyes remained significantly lower through the first month postoperatively. Rabbits receiving MC NLO CXL showed no significant loss of corneal sensitivity.

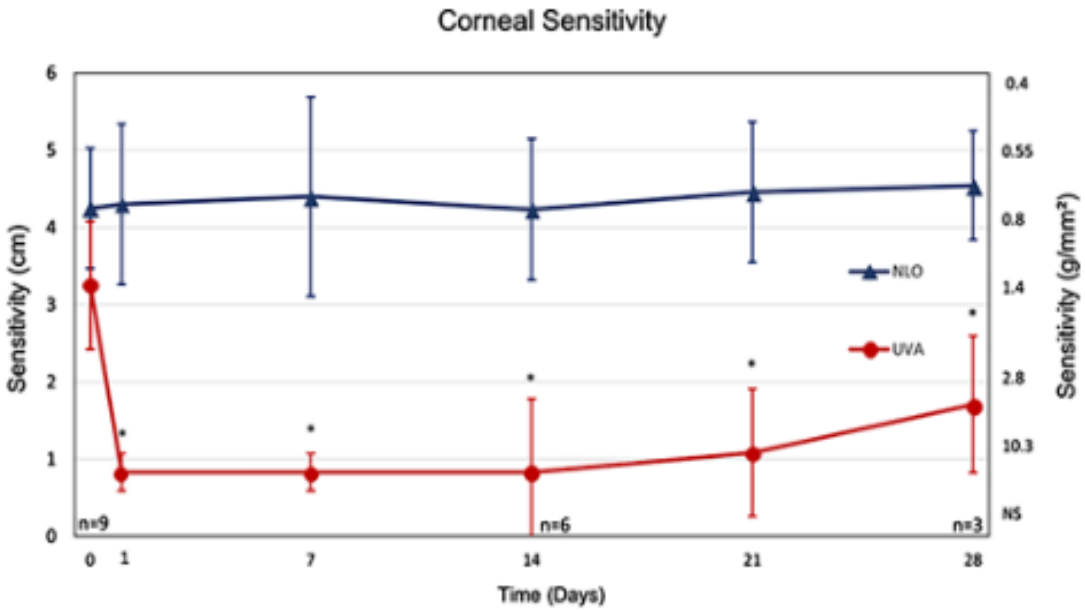

Figure 10: Cochet-Bonnet Aethesiometry

The corneal sensitivity of rabbits was tested over time in both treated and untreated eyes via Cochet–Bonnet aesthesiometry. MC UVA CXL (red) resulted in a significant decrease ($P < 0.05$) in sensitivity, as indicated by asterisks. The sensitivity of MC UVA CXL–treated eyes returned to significantly normal values after day 28. MC NLO CXL (blue) never resulted in any drop in corneal sensitivity.

Furthermore, OCT imaging measurements, as seen in the graphs in Figure 11, revealed that MC UVA CXL–treated eyes exhibited a significant increase in stromal thickness of 232.55 µm and a complete loss of epithelium in the central cornea, both of which returned to baseline values by day 7. MC UVA CXL also resulted in a clear line of demarcation, peaking in depth at day 7 and averaging 236.78 ± 11.88 µm, significantly deeper than all further days. Representative OCT images of MC UVA CXL eyes at each time point can be seen in Figures 11A–E, with arrows representing the depth of the demarcation line (shown at days 1, 7, 14, 28, and 56, respectively). NLO CXL–treated eyes showed no significant change in any thickness value, and no demarcation lines could be seen in any animals at any time point.

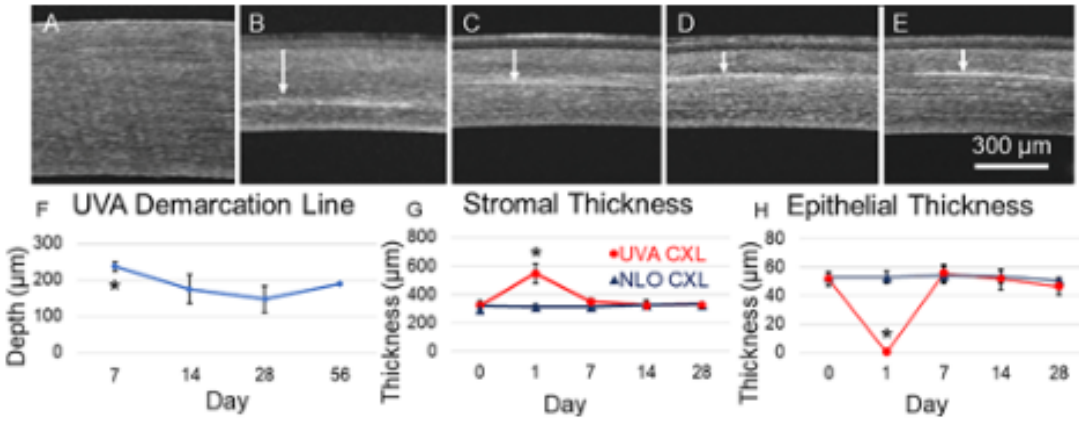

Figure 11: OCT Imaging

Representative OCT images of MC UVA CXL treatment at the time points of 1, 7, 14, 28, and 56 days are shown in A to E, respectively, with arrows denoting the line of demarcation. Graphs show the depth of the demarcation line, stromal thickness, and epithelial thickness over the same time points for both UVA and NLO treatments (red and blue, respectively). MC UVA CXL was shown to result in an increased stromal thickness at day 1 postprocedure accompanied by a total loss of epithelial thickness. MC NLO CXL resulted in no change in either value at any time point. A clear line of demarcation was only observed in MC UVA CXL eyes. Asterisks denote a significant difference of $P < 0.05$.

Image Analysis

CAF was used to confirm that all corneas included in the study contained CXL. We were unable to confirm the region of CXL via CAF in three rabbits within the 2-month NLO CXL group and therefore excluded the results from those animals.

IHC of NLO CXL detected very rare acellular patches within 2-week samples, (Fig. 12A, double arrowhead) and no acellular regions at all at any further time points, indicating cells had already begun migrating back to the area (Fig. 12B). This is consistent with previous data.[20]

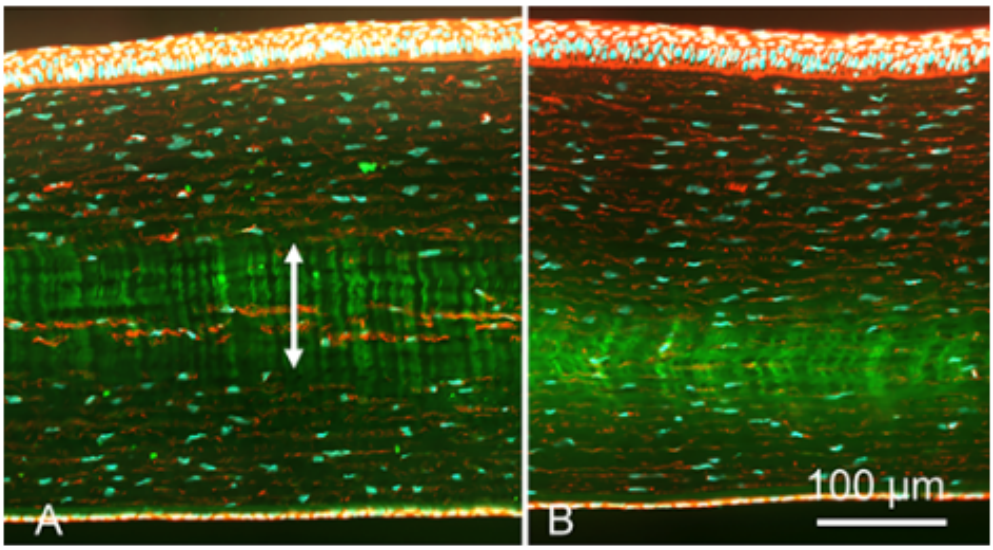

Figure 12: CAF and IHC of MC NLO CXL

After sacrifice, corneas were removed and processed for either IHC or CAF imaging. For IHC, sections were treated with DAPI for staining cell nuclei (cyan) and rhodamine phalloidin for staining actin (red). Cellular staining of MC NLO CXL showed only small, sparse regions of cellular death at 2 weeks (A), while cells had fully migrated back into the region of CAF (green) by 1 month (B).

UVA CXL eyes, however, showed regions of cellular death at all time points (Figs 13B, 13D, 13F), consistent with previous studies.[23] Acellular regions from both procedures corresponded directly with regions of CAF (Figs 13B, 13D, 13F). Analysis of IHC resulted in decreasing depths of acellular zones at each time point, listed in Table 1 as a percentage of the total thickness of the depth measurement of each sample.

Table 1: Demarcation line vs Acellular Zone

Time Point	n	Depth of Demarcation line (%)	Depth of Acellular Zone (%)	Significance
2 Week	3	53.04 ± 11.40	33.43 ± 2.37	**P<0.05**
1 Month	3	43.97 ± 7.12	30.46 ± 3.26	**P<0.05**
2 Month	3	54.50 ± 3.05	25.52 ± 2.24	**P<0.05**

The depth of this region was also significantly shallower than the depths of the demarcation lines measured from the OCT images until the 2-month time point, when

the demarcation line became hard to distinguish at an exact location in any OCT images (Fig 13). Keratocyte density measurements from the IHC images identified lower densities of 636.7 ± 111.01, 686.9 ± 104.68, and 773.0 ± 147.37 keratocytes/mm2 (K/mm2) for UVA-treated eyes at 2 weeks, 1 month, and 2 months, respectively, while NLO-treated eyes showed cell densities of 882.7 ± 113.09, 853.8 ± 117.06, and 957.5 ± 120.57 K/mm2 (Table 2). While cellular densities were higher in NLO CXL eyes at all time points, they were only significantly different at 2 weeks.

Table 2: Cellular Density

Time Point	n	UVA CXL (K/mm^2)*	NLO CXL (K/mm^2)	Significance
2 Week	6	636.7 ± 111.01	882.7 ± 113.0.9	**P<0.05**
1 Month	6	686.9 ± 104.68	853.8 ± 117.06	**NS****
2 Month	3	773.0 ± 147.37	957.5 ± 120.57	**NS**

*Keratocytes/mm^2 **Not Significant

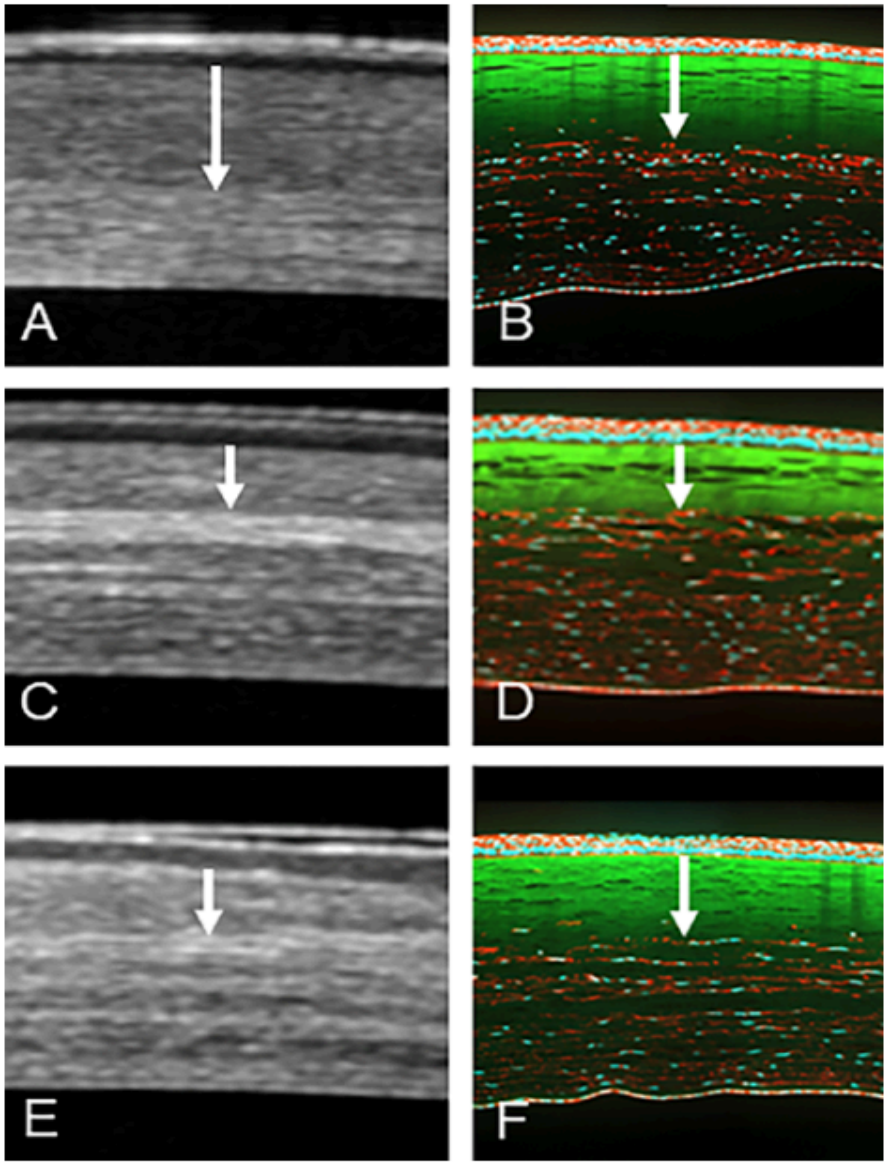

Figure 13: OCT and IHC after MC UVA CXL

In vivo OCT imaging showing representative demarcation lines at the time points of 14, 28, and 56 days (A, C, and E, respectively) with arrows to represent the demarcation line compared to their corresponding IHC within the same animals with arrows to represent depth of the acellular zone. Sections were treated with DAPI for staining cell nuclei (cyan) and rhodamine phalloidin for staining actin (red), with CAF shown in green.

Discussion

Despite traditional UVA CXL being the clinical standard for Keratoconus treatment, its reliance on complete epithelial debridement for optimal Rf stromal delivery is a major drawback - leading to patient pain, a delayed visual recovery, and risk of infection. [40-48] Transepithelial CXL, a novel alternative, still underperforms compared to this treatment due to limited stromal Rf as well as UV light penetration, resulting in ineffective CXL and risk of epithelial damage. [49-53]

FS laser-based epithelial microchannels have been shown to overcome the first obstacle by achieving sufficient stromal Rf concentration required for effective crosslinking while also causing minimal damage to the epithelium. [54-55] NLO CXL is a promising method to overcome the second obstacle by using two photon excitation to precisely control the depth and location of CXL to the laser's focal volume, thus avoiding unnecessary UV exposure to the epithelium and endothelium. The goal of this project was to use an in vivo rabbit model to compare the safety and efficacy from combining epithelial microchannels with either UVA or NLO CXL.

Our first step was to evaluate and optimize the method of Rf delivery. We tested this by varying osmolarities of solutions and examined the effects of UV light transmittance through the methylcellulose-thickened Rf solutions. Changes in Rf osmolarity had a minimal impact on the stromal diffusion - therefore, we used the standard 300 mOsm solution in the following experiments. During treatments, we noticed that corneas that were not rinsed prior to UV irradiation showed minimal collagen autofluorescence (CAF) and cellular damage while the opposite occurred in

corneas that were thoroughly rinsed of remaining Rf. Furthermore, we observed that application of the methylcellulose-thickened Rf solution impeded the transmission of UV - 80% of UV irradiance was blocked by a thickness of 30 μm of Rf solution. We determined that both the epithelium and residual Rf post-dripping acted as a barrier for sufficient UV irradiation into the stroma and resulted in a reduced CXL effect. Going forward, all following in vivo experiments included a PBS rinse in addition to a continued application of Rf (in PBS instead of methylcellulose). We noted that these findings contradict a previous study by Morgan et al. that reported a reduced Rf concentration as well as less effective CXL in corneas that were rinsed prior to UVA exposure; however, their protocol did not include a continued Rf application for the duration of CXL.

We designed the in vivo rabbit portion of this study to overcome the second obstacle - after achieving sufficient Rf stromal saturation, we had to get the UV irradiation through an intact epithelium without injury. The experiment compared the safety and efficacy of MC UVA CXL with MC NLO CXL in both male and female rabbits. We did not observe any sex based differences in the following measurements.

In the MC UVA CXL group, Lissamine green staining showed a complete death of the epithelium that lasted for 3 days. Cochet-Bonnet aesthesiometry revealed a significantly reduced corneal sensitivity for a period of 28 days, indicating nerve damage following the UVA treatment. These results are consistent with previous studies by Xia et al. that showed 90 days were required for complete nerve regeneration and Chen et al. who noted a significant reduction in corneal sensitivity and nerve density following BAK-assisted transepithelial UVA CXL. Imaging results also demonstrated a significant and continued pattern of damage following MC UVA CXL. OCT imaging showed a clear

demarcation line, an increase in stromal thickness, and a significant decrease in epithelial thickness. Furthermore, the depth of the demarcation steadily decreased over time until 1 month after treatment with a similar trend observed for the depth of the acellular zone measured with IHC imaging.

The MC NLO CXL group produced very different results. Following Lissamine green staining, none of the corneas showed a measurable epithelial wound and aesthesiometry showed no change in corneal sensitivity following treatment. These results demonstrate that NLO CXL leaves the epithelium intact and undamaged after the procedure without damage to the superficial nerves. Interestingly, OCT imaging did not reveal any demarcation line and there were no measurable changes in the stromal thickness. Prior to sacrifice, it was uncertain whether CXL had actually taken place due to the absence of any noticeable changes. However, image analysis did confirm CXL in this group. In all but 3 rabbits from the 2 month group, corneal samples showed clear CAF overlapping with regions of cell death. This may be as a result of an off-center crosslinking treatment or the laser being focused too deep into the stroma since all three rabbits were treated on the same day. Imaging of the remaining samples showed a shallower acellular region as well as demarcation line depth. This suggests a strong correlation between cellular healing and the appearance of the demarcation line. The appearance of a demarcation line from other corneal injuries - causing cellular damage and keratocyte activation without CXL - also supports this idea.

This study demonstrates that pairing FS machined microchannels with NLO CXL is a promising transepithelial method that avoids epithelial damage and loss of corneal sensitivity with significantly reduced anterior stromal damage and faster cellular

recovery when compared to MC UVA CXL. By avoiding postoperative patient pain and risk of infection as well as a faster visual recovery, MC NLO CXL produces a safe and effective transepithelial CXL procedure.

Chapter 3: Iontophoresis

Note on Prior Publication

Portions of this chapter have been previously published as:

Joshi, R., Bradford, S. M., Luo, S., Farrah, E., Xie, Y., Brown, D. J., Juhasz, T., & Jester, J. V. (2025). Enhanced riboflavin stromal delivery using microchannel-assisted iontophoresis for corneal crosslinking. *Translational Vision Science & Technology*, 14(3), 18. https://doi.org/10.1167/tvst.14.3.18

Introduction

Keratoconus (KC) and ectasia following corneal refractive procedures-such as keratorefractive surgery (LASIK or surface ablation) or Refractive Lenticule Extraction (RLE)-are characterized by progressive thinning, mechanical weakening of the stroma, and corneal bulging. These conditions can result in visual impairment due to irregular astigmatism and reduced spectacle-corrected distance visual acuity. [56-57] They may also heighten sensitivity to light and cause glare. The etiopathogenesis of KC is complex, and is no longer considered a non-inflammatory disease, as elevated levels of proinflammatory cytokines have been found in the tears and epithelium of KC patients. [58-59] Both genetic and environmental factors seem to contribute to the development of KC, with eye rubbing and a recently identified nocturnal ocular compression playing a role in the pathogenesis. [60-61]

While mild KC can be treated with glasses and contact lenses, more advanced stages may require surgery. [56] For instance, synthetic polymethylmethacrylate (PMMA) intrastromal corneal ring segments (ICRS) are often used to reshape the cornea, reduce irregular astigmatism, and delay the need for more invasive procedures like corneal transplantation. However, their ability to halt keratoconus progression remains debated. [62-63] On the other hand, corneal collagen cross-linking (CXL), which involves soaking the cornea in the photosensitizer, riboflavin (Rf), and exposing it to ultraviolet-A (UVA) irradiation, has been shown to stop or even reverse keratoconus progression. [64] In very advanced cases of keratoconus, penetrating keratoplasty or deep anterior lamellar keratoplasty (DALK)

may be required. [56] However, less invasive anterior keratoplasty techniques-such as Bowman's layer transplantation, corneal allogenic intrastromal ring segments (CAIRS), or intrastromal lenticules-have shown promising results. [65-68] With regard to the most common procedure currently used to slow or halt KC progression, corneal collagen CXL mediated by UVA photoactivation of the Rf and the generation of oxygen free radicals has been shown to induce covalent crosslinks within and between the collagen fibrils and proteoglycan core proteins, resulting in mechanical stiffening and flattening of the cornea. [69-70] In addition to the stiffening effect (up to 300%), crosslinking has been shown to enhance blue collagen autofluorescence (CAF). [71-72] However, as photoactivation of Rf and the generation of oxygen free radicals is cytotoxic and harmful to living tissue, specific parameters for CXL are used to minimize exposure damage to deeper ocular structures such as the corneal endothelium, by limiting the power, treatment time, and concentration of Rf. [72-75]

A major concern about UVA CXL is the method of stromal Rf application. Since the corneal epithelium acts as a barrier to prevent the diffusion of solutes into the stroma, UVA CXL generally requires complete epithelial debridement to ensure sufficient stromal Rf penetration (the Dresden protocol) and effective CXL. This procedure is painful for the patient, requires several days to recover, and increases the risk of microbial keratitis. [71, 74. 76-79] To reduce these side-effects, several alternative approaches have been used, including full-thickness partial mechanical de-epithelization [80-81], multifocal epithelial disruption using a specially designed metallic instrument [82] or a surgical sponge, and partial thickness epithelial removal using excimer laser. [83] Also, to avoid any ocular surface disruption, transepithelial

UVA CXL (TE-UVA CXL) procedures have been proposed that achieve stromal Rf penetration without removing the corneal epithelium**.** Current methods include the addition of chemical excipients such as Benzalkonium Chloride (BAK) or Ethylenediaminetetraacetic acid (EDTA) to loosen epithelial tight junctions. Additions of Glutathione, Vitamins A, C, and E, polyethylene glycol, gentamicin, tetracaine, and corneal iontophoresis during Rf application have also been proposed. [84-91] However, crosslinking as a result of TE-UVA CXL has been shown to be far less effective than traditional UVA CXL. [84, 92-96] This is likely due in part to the reduced Rf penetration into the corneal stroma. The long-term efficacy of this technique compared to the standard epi-off Dresden protocol also has not been determined.

Iontophoresis, a novel method of facilitating TE-UVA CXL, is a noninvasive method where a small electric current is applied to a surface to increase penetration of an ionized substance into the tissue. This method's benefit lays in its ability to provide high drug tissue concentration (50-100x higher concentration compared to passive permeation), [97-98] while minimizing systemic drug exposure. Iontophoresis is used in various fields of medicine including ophthalmology and has been used for transcorneal dexamethasone application post-surgery and methylprednisolone treatment post-PKP to minimize graft rejection. [99-102] Recently, this procedure has been advocated for use in TE-CXL by enhancing intrastromal Rf diffusion while retaining an intact epithelium. [84, 93-96]

The first clinical application of ocular iontophoresis was performed by Wirtz in 1908 to treat serpiginous ulcer of the cornea with 0.5% zinc sulfate using a current of 2 mA

for 1 min. [103] Since then, dyes, antiviral and antibacterial agents, steroids, and genes have been delivered to the eye using this method. Iontophoresis has been lauded for its simple approach requiring only a current generator, an eye cup, and the drug solution as well as providing a non-invasive delivery method that allows the drug to overcome natural permeability barriers. Clinical trials have demonstrated that iontophoresis-assisted CXL is a valid method for treating KC progression but has a far lower efficacy compared to standard CXL. [103-105]

In standard iontophoresis, the Rf is applied with a negatively charged electrode and the circuit completed with an electrode inserted into the vitreous of the eye ex vivo, or the nape or forehead in vivo. The electrode then conducts the current through the corneal tissue. Rf is a great candidate for corneal iontophoresis due to its water solubility, negative charge at physiological pH, and low molecular weight allowing for enhanced penetration. Other variables that influence penetration are the substance's concentration, size, and the application time. Studies have shown that safe and optimal transepithelial iontophoresis of Rf can be achieved using a 1 mA current applied over a duration of 5 mins that can provide sufficient intrastromal Rf concentration for crosslinking stromal collagen. [71, 85, 93] Though these values are clinically used for iontophoresis-assisted CXL and claim to reduce the Rf penetration time from 30 mins to 5-10 min, [73, 93, 104, 106-107] the achieved Rf stromal penetration has been reported to be 2-fold less than the conventional Dresden protocol as shown by Cassagne et al. and Mastropasqua et al. in human donor corneas. [94, 108] We have previously shown that femtosecond (FS) laser based micro-machining of the corneal epithelium to form epithelial microchannels (MC, 2 mm

in diameter and 25 μm deep into the corneal epithelium spaced 50-100 μm apart) can greatly improve passive Rf stromal penetration while also avoiding cellular damage that commonly occurs from addition of BAK/EDTA. [88] Even so, this procedure still requires 30 minutes of Rf application to achieve maximum stromal delivery. [109] The purpose of this study was to determine if iontophoresis when combined with MC for stromal Rf delivery could both shorten the treatment time while also improving Rf stromal delivery by iontophoresis, resulting in more effective CXL.

Methods

Ex Vivo Tissue Preparation

Eighty-four ex vivo New Zealand albino rabbit eyes were shipped overnight (Pel-Freez, Rogers, AK and prepared for experimentation as previously published. [5 ,35, 46] eyes were first rinsed in phenol free, low glucose, Dulbecco's Modified Eagle Medium (DMEM, Sigma-Aldrich, St. Louis, MO) and placed in 12-well tissue culture plates containing sufficient media to cover the sclera up to the limbus. Eyes were then placed in a humidified, 37°C, 5% CO_2 incubator for two hours to restore endothelial pump function and allow the corneal thickness to return to normal. The corneas were then stained with Lissamine Green (10 mg/ml in PBS, Sigma-Aldrich, St. Louis, MO) to verify an intact, damage free epithelium. Eyes with Lissamine green staining, indicating epithelial damage, were discarded. Eyes were then imbibed with a Rf solution with one of three methods: iontophoresis alone [G1], iontophoresis with MC [G2], or MC alone [G3]. Table 3 lists detailed group sizes, Rf solution makeup, and treatment information.

Table 3. Ex Vivo Stromal Riboflavin Delivery and Concentration

Group		Stromal Delivery Method	Eyes (n)	Duration (mins)	Current (mA)	Riboflavin Concentration (ug/ml)
1	A	Iontophoresis	17	10	1	4.73 ± 0.8
	B		5	5	1	4.19 ± 0.42
	C		9	10	0.5	3.65 ± 0.22
2	A	Iontophoresis + Microchannels	17	10	1	12.64 ± 1.82
	B		16	5	1	10.37 ± 2.28
	C		15	10	0.5	12.80 ± 1.37
3	Control	Microchannels	5	30	N/A	13.43 ± 1.15

Microchannels

Epithelial MC were generated using a 1030 nm, 1 kHz, amplified FS laser (One Five Origami, NKT Photonics, Denmark) with a 5 μJ pulse energy adjusted using a polarizing beam cube and half wave plate as reported previously. [5] Using custom Labview software, the FS laser beam was focused to precisely cut to a 25 μm deep, 2 μm diameter channel with 50 μm spacing over the central 6mm diameter area of the cornea. This procedure results in ~10% of the corneal surface having MC. As previously published, this approach produces sufficient stromal Rf penetration for corneal crosslinking without damage to the corneal epithelium. [5, 35, 46]

Iontophoresis

The basic setup for iontophoresis is shown in Fig 14 and involves the use of a constant current source (A) from OPIA Technologies (Iontofor-CXL) and two electrodes. The anode (B, return electrode) was a sterile 18-gauge needle inserted

into the vitreous chamber (ex vivo) or the rabbit's neck (in vivo) while the cathode (C, main electrode) was a stainless steel mesh enclosed in an 8 mm diameter circular cup with a surrounding 1 mm wide annular suction ring that attaches the device to the cornea secured by a vacuum syringe (D) for the duration of the iontophoresis treatment. The cathode was placed 8 mm away from the cornea to allow air bubbles to escape from the side. The mesh reservoir in the cathode was filled with a topical Rf solution (1.0% riboflavin-5-phosphate in PBS, Sigma-Aldrich, St. Louis, MO) with optimized osmolarity for penetration (300 mOsm/L) which also acts as contact between the cornea and electrode. When treatment begins, the current generator (A) outputs a constant direct current (0.5 or 1 mA) for a set period of time (5 or 10 min). Voltage fluctuations during treatment were monitored using a digital multimeter to maintain a 3 to 5V range. Rf was suctioned out with the extra syringe and fresh solution was applied for each eye.

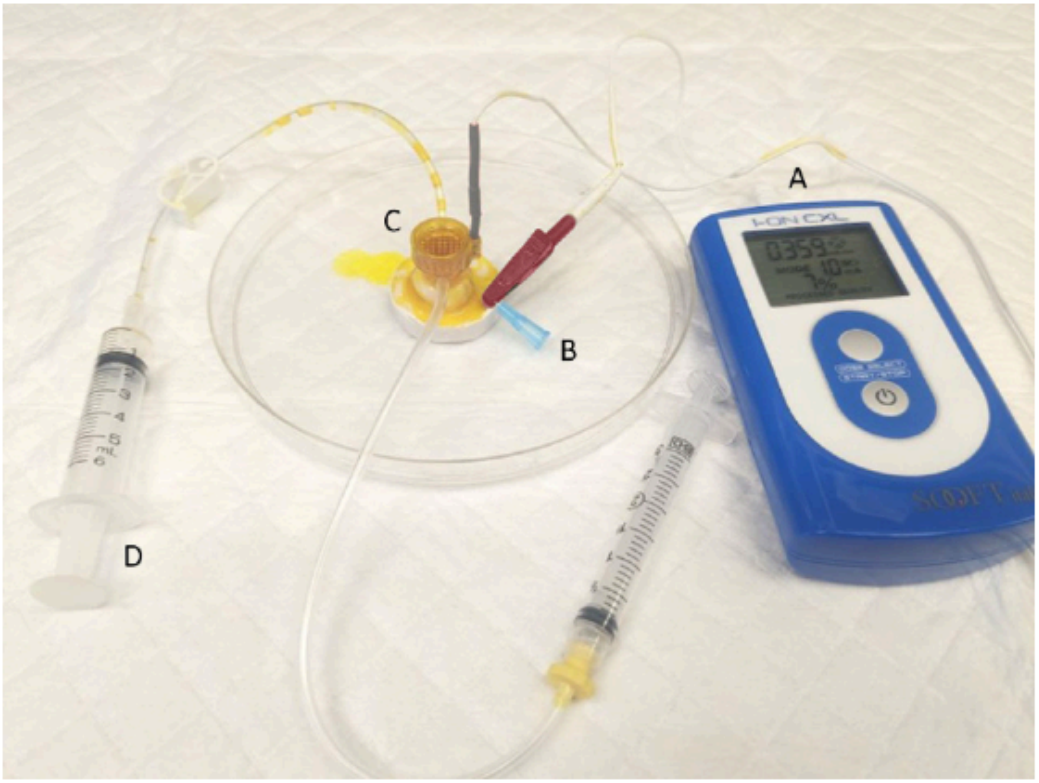

Figure 14: Iontophoresis Rf Delivery

Iontophoresis riboflavin delivery system modified for use in ex vivo eyes. The constant current source (A) is connected to the positive electrode (B), a 22-gauge needle is inserted into the vitreous chamber, and the negative electrode (C) containing the riboflavin solution is submerging the stainless-steel grid. The annular suction ring is secured by the vacuum syringe (D) to steady the device during the procedure.

Experimental Design

The 84 ex vivo rabbit eyes were divided into three treatment groups as shown in Table 3. The first two groups (G1, iontophoresis alone, 31 eyes) and (G2, iontophoresis with MC, 48 eyes) received Rf iontophoresis using three different settings of: 1 mA for 10 min [A] (G1: n = 17, G2: n = 17), 1 mA for 5 min [B] (G1: n = 5, G2: n = 16), and 0.5 mA for 10 min [C] (G1: 9, G2: 15). These variations were chosen to determine the treatment which maximized stromal Rf penetration while minimizing

current and treatment time. The last group (G3: n = 5) received MC alone and was used as a control.

Measuring Stromal Riboflavin Concentration

Measurements of stromal Rf concentration were performed as previously published. [46] Briefly, excess Rf was wiped with cotton gauze and the epithelium removed with a Tooke knife. Using a 6 mm trephine, a central corneal button was cut out and then placed in 1 ml of PBS solution overnight to allow the Rf to elute from the button. This process was done quickly (3 minutes from cutting to depositing in PBS) to avoid loss of Rf into the anterior chamber. The weight of the solutions were measured before and after addition of the button to account for any variance in sample volumes.

After 24 hours, the Rf concentration of the eluate was measured with a spectrophotometer (Spectramax Gemini XPS microplate reader, Molecular Devices, CA) with 380 nm excitation and 540 nm emission. Serial dilutions of the Rf solution were made and used to create a standard curve for the calculation of Rf concentration (ug/ml) which was used to quantify each sample's measured intensity values.

Live Rabbit Model

A total of 6 New Zealand albino rabbits (4-5 months old) were used in this study and sacrificed 24 hours after treatment. All animals were treated according to the ARVO statement on the use of animals in vision research, and experiments were approved by the IACUC of the University of California, Irvine (AUP 23-016). Only the right eye of each of the rabbits was treated in our experiment.

Surgery

Rabbits were split into two groups of 3 each and treated with a current of 1 mA for a duration of 5 min. These values were chosen as they have been used extensively and are the current clinical standard for iontophoresis-assisted crosslinking. [39-40, 42, 45, 47, 49, 52-53, 57] The first group underwent iontophoresis alone while the second group received iontophoresis with MC. Prior to treatment, all animals were anesthetized with a subcutaneous injection of 30 to 50 mg/kg of ketamine hydrochloride (Zoetis, Parsippany-Troy Hills, NJ) and 5 to 10 mg/kg of xylazine (Akorn, Lake Forest, IL). Each rabbit was set in a rabbit restrainer with a speculum positioned on the eye. Each cornea had a baseline line anterior segment scan taken with an OCT (DRI OCT Triton plus, Topcon,
Japan).

After Rf treatment, UVA CXL was performed using the previously described protocol. [56] Rabbits then received a drop of 0.5% tetracaine hydrochloride (Alcon, Ft. Worth, TX) to prevent pain. Post-treatment each rabbit received 0.1 to 1 mg/kg of Revertidine (Modern Veterinary Therapeutics, Miami, FL) to reverse the sedative and 0.1 ml of buprenorphine hydrochloride (0.3 mg/ml, Reckitt Benckiser Healthcare, UK) for analgesia. Additionally, each rabbit was given a drop of 0.3% gentamicin (Allergan, Irvine, CA) in the treated eye three times in the next 24 hours after treatment to prevent infection.

Sacrifice

After 24 hours, another OCT image was taken of each eye and then the treated rabbit corneas were stained with Lissamine green to determine the extent of epithelial damage and euthanized with an intravenous injection Euthasol (1 ml, Virbac AH, Fort Worth, TX) into the marginal ear vein. Immediately after death, the corneas were fixed in situ under 20 mm Hg pressure via perfusion of 2% PFA (Mallinckrodit Baker, Inc., Phillipsburg, NJ) in PBS at 4°C to maintain the in vivo collagen structure. They were then removed and fixed overnight.

CAF Imaging

To verify and quantify the degree of CXL using blue collagen autofluorescence (CAF), corneas from in vivo experiments were embedded in 10% low melting point agarose (Lonza, Rockland, ME) and sectioned along the superior-inferior meridian into 200 micron thick sections using a vibratome (Campden Instruments, Loughborough, England). The samples were then imaged for blue CAF using a Leica Stellaris 8 multiphoton confocal microscope with a Chameleon FS laser (Coherent, Santa Clara, CA) as the excitation source. The samples were excited at 760 nm and the CAF signal was collected between 400 and 450 nm using a 20x objective. Images of the central cornea were exported to an image analysis software program (Metamorph, Molecular Devices, Sunnyvale, CA) and three 100 x 100 pixel (100 pixels = 25 μm) areas in the central anterior crosslinked region and posterior stroma (background region) were identified in 3 sections for each cornea. The first 100 x 100 region was placed in the center of the CAF region in the anterior stroma with the other

two 100 x 100 regions placed adjacently. This process was repeated in the posterior of the stroma to determine the background. The average intensity within both regions were subtracted to identify the average CAF value in the anterior of the cornea (CAF_{ANT}).

The depth of crosslinking was also measured by generating three regions through the center of the cornea extending from the anterior to posterior of the stroma. We then used a line scan to calculate the mean fluorescence intensity along each line, measured the background intensity, and plotted this as a function of corneal depth - showing the change in pixel intensity from the anterior to posterior stroma. By integrating the area under this depth-intensity curve (CAF_{AUC}), we estimated the total CAF between both groups. Peak pixel intensity was determined by looking at the maximum intensity value in the AUC plot for each group. CXL depth (CAF_{depth}) was determined by noting the distance from the beginning of the intensity signal to the point where the intensity signal equaled the background intensity. This distance was divided by the thickness of the section from anterior to posterior stroma and was expressed as a percent thickness of the section.

Statistics

Statistical analysis was performed in statistical software SigmaPlot (SPSS Inc.,Chicago, IL) using the Tukey-Kramer method for a multiple comparison, one-way analysis of variance (ANOVA). Groups were considered to have a statistically

significant difference with a p-value less than 0.05. Error bars represent the standard deviation in all following figures.

Results

Effects of Iontophoresis on Stromal Rf Concentration in Ex Vivo Rabbit Eyes

Table 3 and Fig 15 show the measured stromal Rf concentrations achieved in ex vivo eyes using the various treatment protocols. Corneal button weights between samples and treatment days were consistent. Iontophoresis alone (G1, n = 31) achieved Rf stromal concentrations of 4.73 ± 0.82 ug/ml (1 mA for 10 min), 4.18 ± 0.42 ug/ml (1 mA for 5 min), and 3.65 ± 0.23 ug/ml (0.5 mA for 10 min. In this group, 0.5 mA treated corneas for 10 min achieved significantly lower Rf concentration than 1 mA for either 5 or 10 min. The same iontophoresis exposures combined with MC (G2, n = 48) achieved a 3+ fold higher ($P < 0.001$) Rf concentration averaging 12.64 ± 1.82 ug/ml, 10.37 ± 2.28 ug/ml, and 12.8 ± 1.38 ug/ml for the same iontophoresis protocols stated above. Iontophoresis with MC when performed at 1 mA for 5 mins was significantly lower than both 1 mA and 0.5 mA for 10 minutes but remained significantly higher than iontophoresis alone. Furthermore, iontophoresis with MC for 10 minutes at 0.5 or 1 mA achieved equivalent stromal concentration of Rf as MC alone (G3, n = 5) after 30 minutes of Rf treatment ($p > 0.05$).

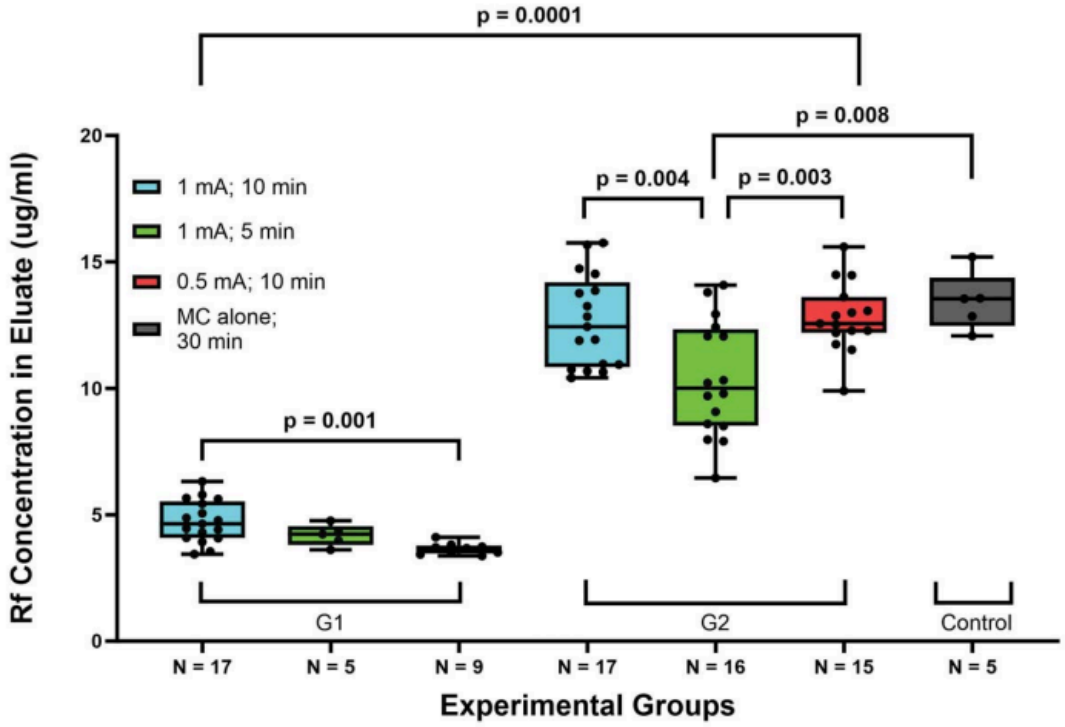

Figure 15: Effects of Iontophoresis with or without MC on Rf Concentration

Penetration graph of Rf stromal concentration 24 hours after procedure. The treatment groups: group 1 = iontophoresis alone, group 2 = iontophoresis + MC, and the control group (MCs for 30 minutes) are compared and show average ± SD for each variable iteration.

In Vivo Efficacy of UVA CXL

In vivo OCT images taken at baseline and post-CXL (1 Day) were used to measure changes in stromal thickness using Metamorph after iontophoresis alone and iontophoresis with MC (Fig 16, A and B respectively).

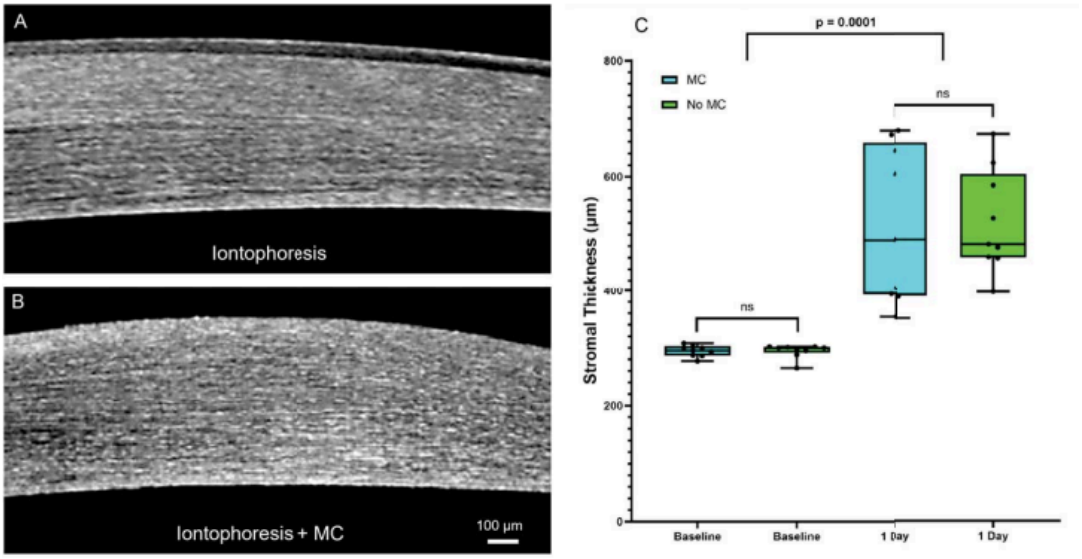

Figure 16: OCT Imaging of Treated Corneas

Representative images taken 24 hours post-treatment show significant stromal swelling in both the iontophoresis alone (A) and the iontophoresis + MC (B) groups. There was no significant difference between groups at baseline and at 24 hours (C).

Post-treatment, the stroma was significantly increased ($p = 0.0001$) after iontophoresis alone, swelling 73.22% (294.67 ± 3.29 µm to 510.44 ± 90.41 µm) and 69.86% following iontophoresis + MC (294.56 ± 5.70 µm to 500.33 ± 72.63 µm) which were not significantly different (Fig 3C). Lissamine Green staining (Fig 17) revealed a significantly ($P = 0.0001$) higher area of epithelial damage in the iontophoresis + MC group (23.87 ± 5.49 mm^2) compared to the iontophoresis group (1.03 ± 0.97 mm^2). Quantification of epithelial wound dimensions was performed using the open-source software QuPath by measuring the area of the LG stain before and after the procedure.

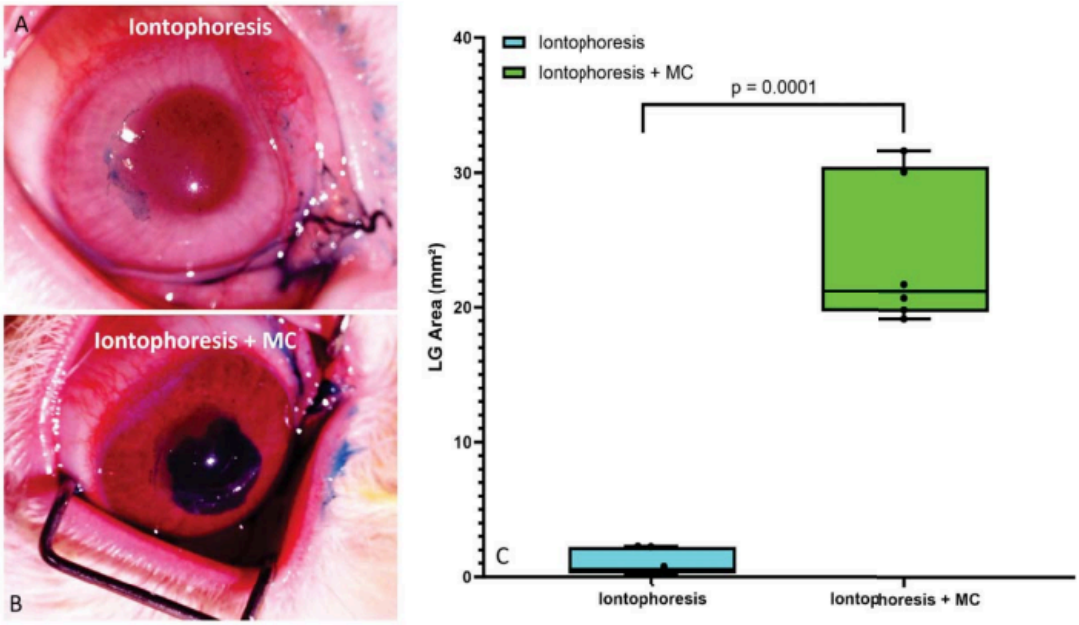

Figure 17: Corneal Lissamine Green Staining

Images taken 24 hours post-treatment of rabbit eyes stained with Lissamine Green to show the extent of corneal damage. Eyes treated with iontophoresis alone (A) showed an average of 4.08% of the epithelium being damaged, whereas those treated with iontophoresis + MC (B) showed a significantly higher loss of (94.98%, P = 0.0001).

Collagen Autofluorescence

A graphical and numerical comparison of the in vivo CAF area under the curve (CAF_{AUC}), average anterior stromal CAF accounting for background intensity (CAF_{ANT}), and crosslinking depth (CAF_{depth}) are shown in Fig 18 and Table 4.

Table 4. Collagen Autofluorescence and Depth of Crosslinking

Treatment	n	Peak Intensity (A.U.)	Total CXL = CAF_{AUC} (A.U.)	Anterior CAF = CAF_{ANT} (A.U.)	CXL Depth = CAF_{depth} (%)
Iontophoresis	3	30	6512 ± 169	23.38 ± 1.49	45.21 ± 1.36
Iontophoresis + Microchannels	3	165*	23151 ± 289*	96.31 ± 4.47*	51.19 ± 4.52

*Peak intensity, CAF_{AUC}, and CAF_{ANT} values in iontophoresis + MC group were significantly higher (P = 0.0001) than iontophoresis alone

**AUC = area under the curve

In G1 (iontophoresis alone), there was a peak CAF (maximum pixel intensity in AUC graph) value of 30 A.U, total CAF area of 6512 ± 169 A.U., and an average anterior stromal CAF (CAF_{ANT}) in the crosslinked region of 23.38 ± 1.49 A.U. G2 (iontophoresis + MC) had respective values of 165 A.U., 23151 ± 289 A.U., and 96.31 ± 4.47 A.U. Iontophoresis with MC (G2, with MC, n = 3) achieved a significantly higher (4-fold) than iontophoresis alone but both groups showed a similar CXL depth (CAF_{depth} - 51.19 ± 4.52% vs 45.21 ± 1.36% respectively).

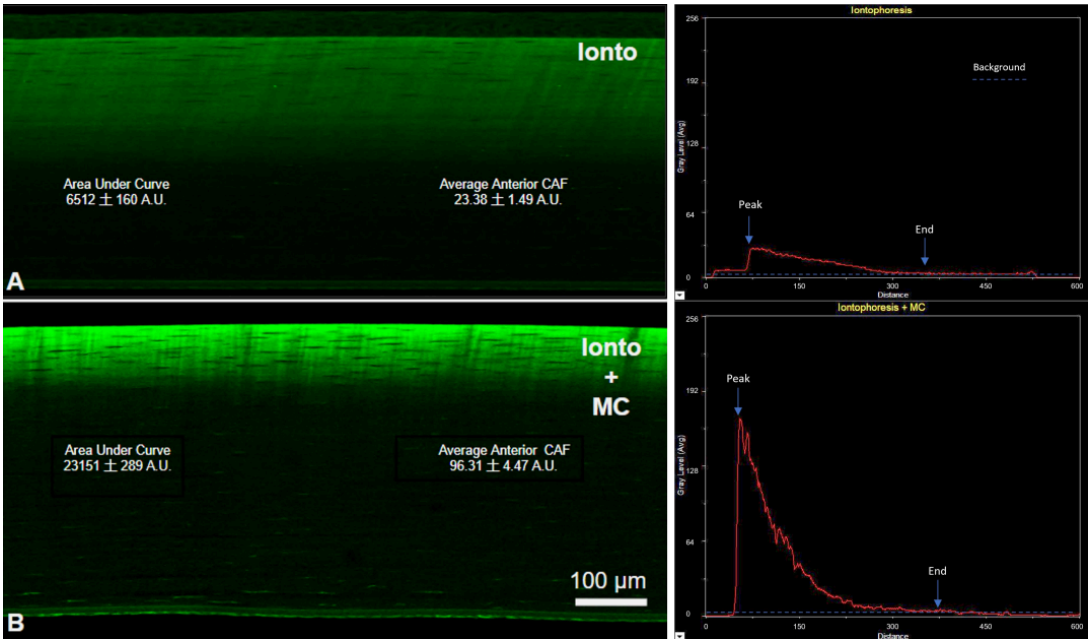

Figure 18: Corneal Collagen Autofluorescence (CAF)

Collagen autofluorescence from representative samples of the two experimental groups (A) iontophoresis alone and (B) iontophoresis with MC, both using 1 mA for 5 minutes. Iontophoresis achieved an average CAF value of 23.38 ± 1.49 AU with a total crosslinked area of 6512 ± 160 AU, whereas iontophoresis + MC achieved significantly higher metrics (96.31 ± 4.47 AU and 23151 ± 289 AU, respectively).

Discussion

Though there have been several transepithelial studies to try and replicate the success of the traditional epi-off method, none have been able to achieve the same degree of crosslinking. [90, 92, 94-98] Though the addition of chemical excipients such as BAK and EDTA facilitates Rf penetration into the stroma through loosening of the epithelial tight junctions, they also increase patient pain and delay post-op recovery similar to standard epi-off CXL. [46, 61. 69-71, 83] Excimer laser use prior to CXL has also been studied. In a clinical study [79] Bakke et al. compared postoperative pain severity and riboflavin penetration rates between two corneal crosslinking (CXL) methods: excimer laser superficial epithelial removal and

mechanical full-thickness epithelial removal and concluded that excimer laser superficial epithelial removal led to greater postoperative pain and a longer riboflavin application time to achieve corneal saturation.

Additionally, in a recent experimental study [98] Brekelmans et al. evaluated the efficacy of corneal cross-linking (CXL) and chromophore penetration (Rf and Rf with 20% Dextran both at 0.1% and WST11 and WST11 with 20% Dextran both at 2.5%) after excimer laser-assisted patterned de-epithelialization in porcine eyes and showed that all chromophores induced significant CXL with similar stiffening across formulations and de-epithelialization methods. Light transmittance was lower after full de-epithelialization, but stromal chromophore penetration was comparable between methods. The researchers concluded that excimer laser-assisted patterned de-epithelialization enabled effective CXL, but reduced chromophore concentration may impact UVA attenuation safety.

One of the major reasons for these poor results from transepithelial attempts is insufficient Rf penetration and lack of stromal saturation during UV irradiation. Our study establishes that iontophoresis when combined with MC, can lead to a dramatic four-fold increased Rf concentration within 10 minutes of application compared to iontophoresis alone and equivalent to MC alone for 30 mins. Intrastromal Rf concentration is a major factor determining CXL efficacy. To date, most iontophoresis studies have used a 0.1% hypo-osmolar Rf solution usually paired with excipients such as BAK/EDTA/Trometamol to enhance penetration into the stroma despite an intact epithelium. Unfortunately, this method's low stromal Rf saturation does not result in sufficient crosslink formation for the treatment to be effective, nor does it

address the issue of post operative patient pain. With our combined iontophoresis + MC delivery system - though results are less than that achieved by complete epithelial removal – we were able to achieve a higher level of stromal Rf concentration through enhanced Rf diffusion without de-epithelialization and addition of excipients. Additionally, UVA photoactivation of Rf following iontophoresis + MC achieved an in vivo CAF level that was nearly 4x that of iontophoresis alone while shortening the Rf application time from 30 to 5-10 minutes. Despite not removing the epithelium and avoiding the addition of BAK/EDTA, the iontophoresis+MC treatment resulted in the complete death of the epithelium showing that this method does not mitigate the risk of patient pain.

There are a few notable points to discuss from our results. First, that the MC procedure by itself does not induce a complete death of epithelium – it damages a very small portion of the epithelium and the damage is hardly visible after only 3 hours of culture. The death of the epithelium is not from the manner of Rf penetration but due to the UVA irradiation post MC generation. This can be seen by the fact that the corneal epithelia remained intact after UVA irradiation post iontophoresis alone, but not when MCs were added. Not only do these results match what we have seen in our previous work [15, 50, 96], but other groups have also seen similar results in in vivo rabbit and ex vivo porcine corneas as well as in human clinical trials. Slit lamp exams, immunohistochemistry, topography readings, OCT imaging, and patient testimonies indicate that iontophoresis CXL with Rf solutions ranging from 0.1% (single dose) to 0.25% (double dose) without the addition of chemical excipients causes little or no change in pachymetry, endothelial cell damage, or other aberrations - suggesting

maintenance of an intact epithelium after the procedure. [21, 97-99] Patients pain reports were also few and superficial. In contrast, patients and eyes subjected to iontophoresis CXL with addition of excipients or laser ablation showed comparable epithelial and stromal damage to Dresden protocol CXL with epithelial debridement but displayed greater improvements to Kmax, BCVA, flattest and steepest meridian keratometry, corneal astigmatism, aberrometery, and central corneal thickness after 6, 12, and 24 months – though not at the level of standard epi-off UVA CXL. [23, 100-101] We infer that iontophoresis alone without the aid of excipients or laser ablation causes little to no epithelial damage but also results in a markedly lower CXL effect. This is reflected clinically by a higher percentage of patients treated with iontophoresis CXL requiring a second CXL treatment 6 months afterward or other form of visual aid (Intacs, scleral lenses, glasses, etc.) than those that underwent iontophoresis + excipient, epi-off iontophoresis, or standard epi-off UVA CXL. [101-106]

In conclusion, iontophoresis when paired with MC allows for a much higher rate of Rf diffusion into the corneal stroma before UVA treatment that is sufficient for the formation of collagen crosslinks at a level equivalent to traditional UVA CXL. When compared to iontophoresis alone, stromal Rf penetration was tripled and CAF was four-fold greater. These values are consistent with those reported in studies where investigators report a 50% effect of iontophoresis alone when compared to epi-on UVA CXL. Further studies are possible with iontophoresis parameter variability (accelerated crosslinking) and modification of the Rf solution makeup and concentration. The greatest benefit of this iontophoresis + MC technique would be in

conjunction with our NLO CXL (nonlinear optical crosslinking) treatment. This method uses a two photon method of Rf activation as opposed to the single photon utilized by UVA CXL. With NLO, activation (and therefore crosslinking) only occurs within the focal volume of the laser which can be set to any depth and scanned through any pattern, allowing for crosslinking of regions below the epithelium without affecting the epithelium at all, leading to a faster and more precise CXL.

Chapter 4: Tenascin-X KO

Introduction

Tenascin-X (TNX) is an extracellular matrix glycoprotein that maintains the integrity of the collagenous matrix. TNX deficiency is one of the causes of Ehlers-Danlos syndrome (EDS) which causes hypermobility of joints, hyperextensibility of the skin, chronic pain, cardiovascular issues, etc. In ophthalmology, EDS is known to lead to ocular conditions such as Keratoconus (KC).

TNX is expressed primarily in the corneal stroma and limbal basal epithelium and is known to decrease the density of collagen fibers in TNXKO mice. The goal of this study was to determine if TNX causes any change in the corneal keratocyte density or stromal collagen organization.

Methods

Tissue Preparation

After receiving the 28 eyes (14 WT and 14 TNXKO at 8W, 1Y, and 2Y), they were placed in 2% paraformaldehyde (PFA) and stored at 4°C. The following day (24 hours later), they were separated into groups. Half of the eyes were used for immunohistochemistry (IHC) while the other half were evaluated for collagen organization using second harmonic generation (SHG).

IHC

A 1.5mm corneal trephine was used to cut a button from the center of each cornea. Each button was initially washed (3 x 30 min) with 50% TD buffer at 4°C on a rocker and then stained with a) DAPI (1:2000) to detect and count keratocyte nuclei and b) 1:10 Phalloidin (Alexa Fluor 555, Thermo Fisher Scientific, Waltham, MA, Cat #: A30106) to visualize the actin cytoskeleton. After staining for 72 hours (3 days) at 4°C followed by 3 x 30 min washes in 50% TD buffer at 4°C on a rocker, each button was mounted on a glass slide with 50% glycerol epi-side-up and imaged using a Leica Stellaris 8 (Leica Microsystems, Wetzlar, Germany) confocal microscope with a 20x dry objective and a lateral resolution of 0.40 microns per pixel. Z stacks containing 512 x 512 image planes extending from the epithelium to the endothelium in 2 µm steps were taken in three regions of the button.

The software Imaris (Oxford Instruments, Abingdon, United Kingdom) was then used to visualize and analyze each button. Using the in-built machine learning model, we trained the software to detect, outline, and count the nuclei in the region of the 3D Z stack for each sample (Fig 19A and 19B). Keratocyte counts of samples from the same button were averaged to perform statistical analysis to determine differences in keratocyte density between mouse ages (8W vs 1Y vs 2Y) and mouse type (WT vs TNXKO). GraphPad Prism (GraphPad Software Inc., San Diego, CA) was used to run a Two Way Anova with the same software being used to determine significance and plot the results.

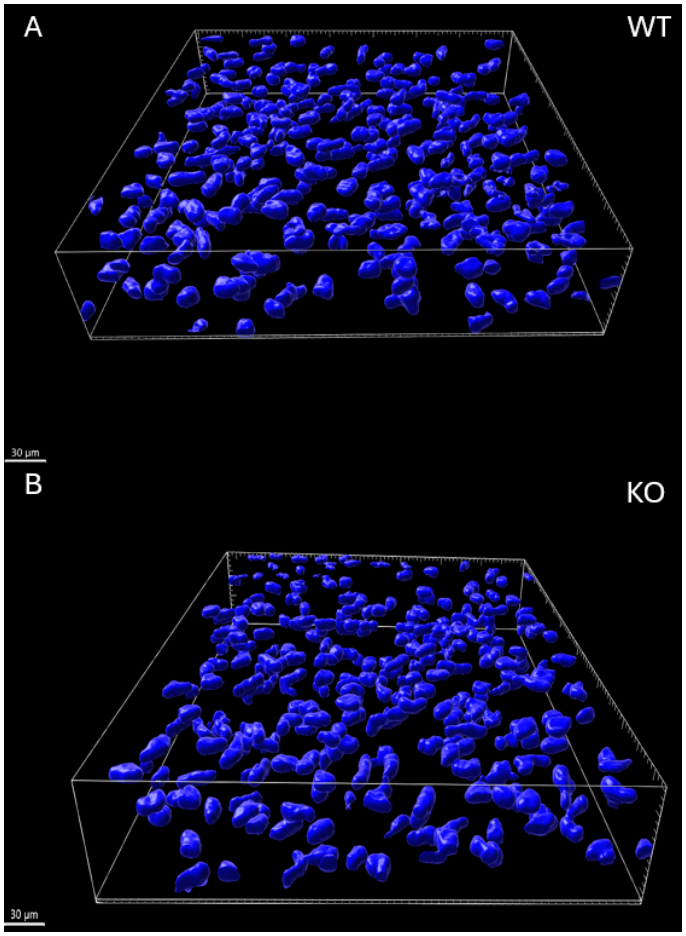

Figure 19: Identification and Quantification of Corneal Keratocytes

The software Imaris was used to train a machine learning model to detect, identify and count positive keratocytes (blue) in the volume of the corneal button using size, shape, volume, and intensity parameters.

SHG

Each cornea was embedded in 20% agarose. A Leica VT1200S (Leica Biosystems, Nussloch, Germany) was used to cut 100 micron serial vibratome sections in the center of each cornea. These sections were stored in phosphate buffered saline (PBS) until they were imaged.

For imaging, we used the Leica Stellaris 8 confocal microscope. SHG signals were generated to determine differences in stromal collagen organization. This was performed by tuning the Chameleon (Coherent, Inc., Santa Clara, CA) laser to 820 nm and collecting both the forward and backward scatter signal. As before, we collected 3D image Z stacks in three regions per section and 2-3 corneas were analyzed per time point and mouse strain. In both IHC and SHG corneas, microscope settings were kept constant for the entirety of the experiment (exposure time, scan time and speed, pinhole size, gain, etc). Peak pixel intensity measurements were used to determine the forward to backscatter ratio for each group.

Stromal collagen angular displacement was assessed using ImageJ's (Fiji, University of Wisconsin, WI) Directionality and OrientationJ plugins as we had done before [108]. Stromal thicknesses for all corneas consistently ranged between 90 and 110 microns, so a cutoff point was chosen at the mid-stromal thickness for each dataset. Each image plane was separated into anterior and posterior regions (Fig 20A), expanding on a method we had used previously [109]. Next, three 25 by 25 μm sub-regions were created within each anterior and posterior region. Using ImageJ, an orientation map and histogram were then generated to display the directions of the collagen fibers in each image plane of the Z stack for each image plane. The histogram showed the full range and frequency of angles within each section. The orientation map - using ImageJ's native Fourier filter to create lines of direction at points of highest pixel intensity - colored the image according to its local directionality (Fig 20B), highlighting collagen fibers of highest intensity. Furthermore, this tool assessed and quantified the

collagen alignment within the subregion and reported this signal between -90° and 90° with respect to the X-axis. This allowed us to measure the angular offset between the adjacent stromal collagen lamellae and repeated throughout the entire 3D dataset. Angular measurements (direction) and deviation from center of Gaussian distribution (dispersion) were recorded and the average and standard deviation were calculated separately between the anterior and posterior regions from their respective three subregions.

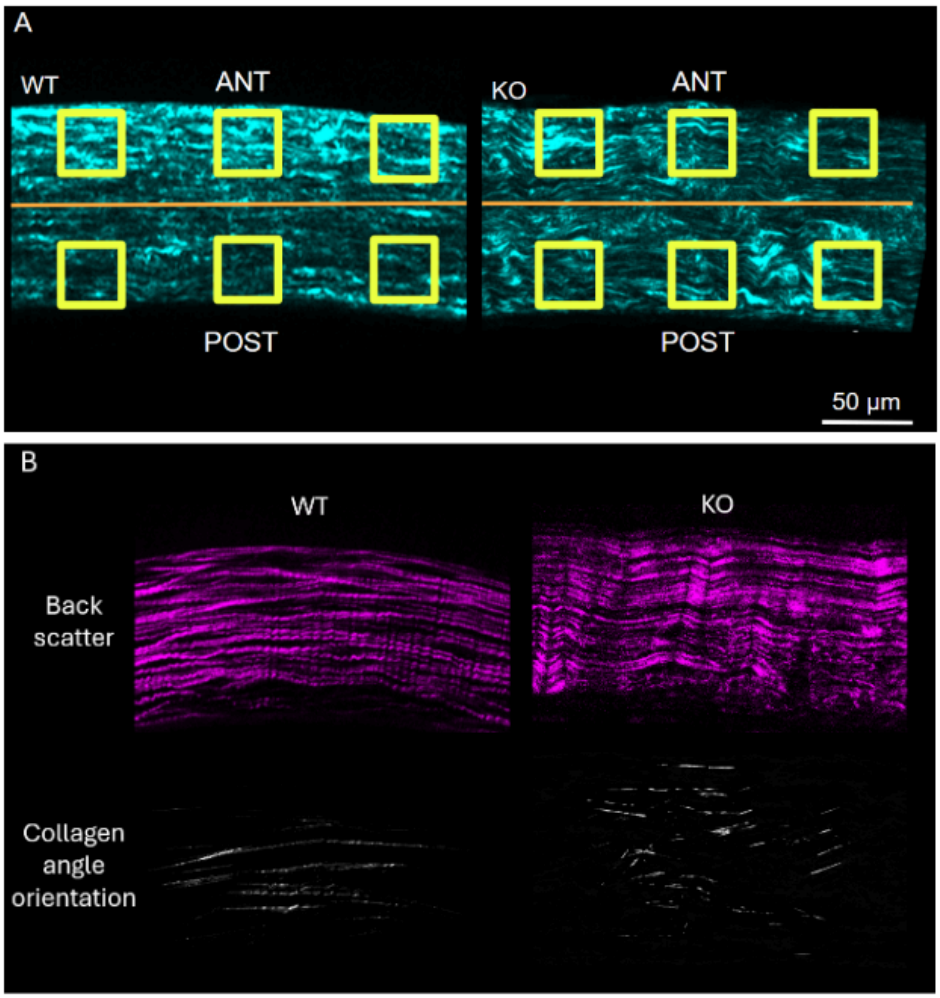

Figure 20: Mouse Corneal Imaging and Orientation Measurements

The corneal stroma was divided into anterior and posterior regions. Three 25 x 25 µm boxes (A) were created in each region to measure angular offset

between adjacent lamellae and averaged to identify a singular value per slice. Angular measurements were performed on each region (B) using ImageJ's Directionality and OrientationJ plugins to quantify the collagen's angular alignment within each subregion and report these angles between -90° and + 90° w.r.t the X-axis. These values were used to determine collagen direction and dispersion.

Statistics

From the through-focus datasets of each mouse strain and time point, keratocyte count, angular measurements and angular dispersion underwent statistical analysis with GraphPad Prism using the Tukey-Kramer method for a repeated measures 2-way analysis of variance (ANOVA). Groups were considered having a statistically significant difference with a P-value less than 0.05. The resulting fiber orientation statistics were then plotted with the same software.

Keratocyte density for the different groups and timepoints can be seen in Fig 21. Mean nuclei counts (cells/mm^3) for the WT (n = 3) at each time point (8W, 1Y, 2Y) were as follows: 27837 ± 1686, 26806 ± 2675, 28512 ± 1132). The respective TNXKO (n = 3) nuclei counts (cells/mm^3) were 27363 ± 2882, 30248 ± 587, 27808 ± 725.

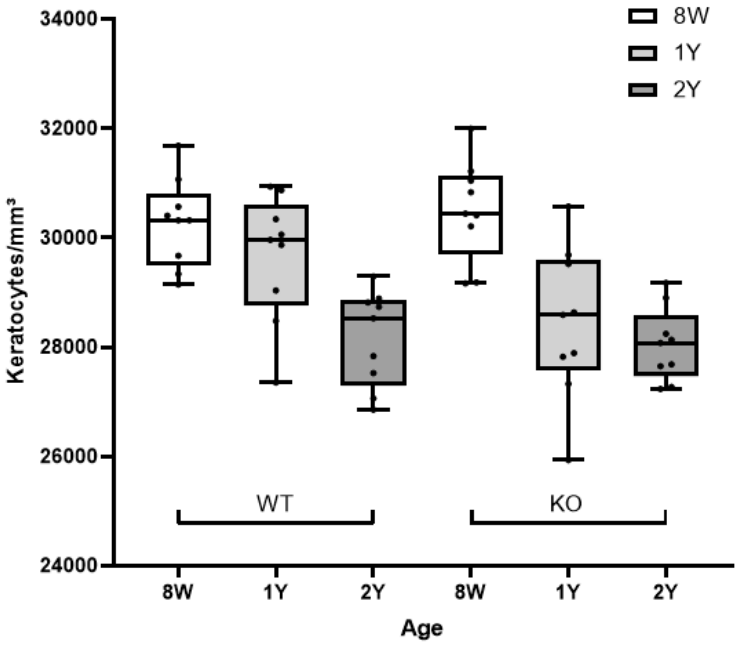

Figure 21: Nuclear Density in WT vs TNXKO Corneas

Comparison of corneal nuclear density between WT and TNXKO corneas at 8W, 1Y, and 2Y. There were no significant differences with respect to mouse strain (WT vs TNXKO) or time (8W vs 1Y vs 2Y).

Differences in range in collagen angles between WT and TNXKO at each time point can be seen in Fig 22A and 22B. In the anterior region of the stroma, the variation in collagen fibrillar angles (Fig 23) for WT corneas (n = 3 per time point) ranged between -3.66° to 8.28° (± 9.21°), -2.33° to 10.86° (± 12.20°), and -2.79° to 9.21° (± 10.20°) for 8W, 1Y, and 2Y respectively. For TNXKO (n = 3 per time point), the respective collagen fibrillar variations ranged from -12.08° to 16.44° (± 13.75°), -10.26° to 18.93° (± 14.11°), and -11.44° to 11.86° (± 13.59°). In the posterior of the stroma, the corresponding values were -2.41° to 2.72° (± 6.49°), -2.02° to 3.11° (± 5.20°), and -4.02°

to 4.11° (± 3.49°) for WT corneas and -2.77° to 3.59° (± 6.01°), -1.89° to 2.88° (± 6.01°), and -3.48° to 2.75° (± 5.81°) for TNXKO corneas.

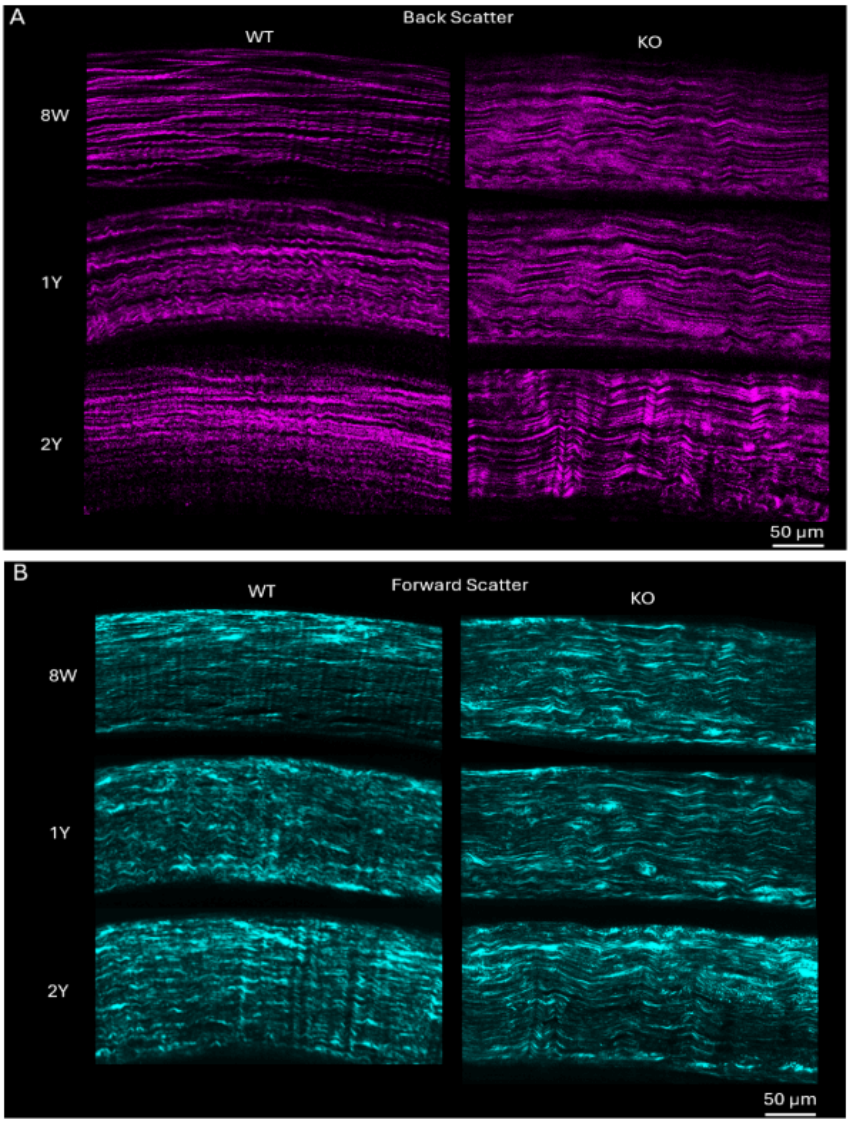

Figure 22: Changes in Corneal Collagen Organization over Time

In both the SHG backscatter (A) and forward scatter signals (B), there are little to no observable or measurable change in the WT group whereas the fibers become increasingly angled and disorganized in the TNXKO group. The ratio of forward to backscatter was 2:1 for both WT and TNXKO groups.

Variation in collagen fiber angular dispersion can be seen in Fig 5B. In the WT strain at each time point (8W, 1Y, 2Y), the mean angular dispersion values were as follows: 3.51° ± 1.98°, 2.68° ± 1.1°, and 5.85° ± 1.21°. The respective values for TNXKO were as follows: 14.39° ± 3.90°, 11.36° ± 3.03°, and 16.67° ± 4.05°.

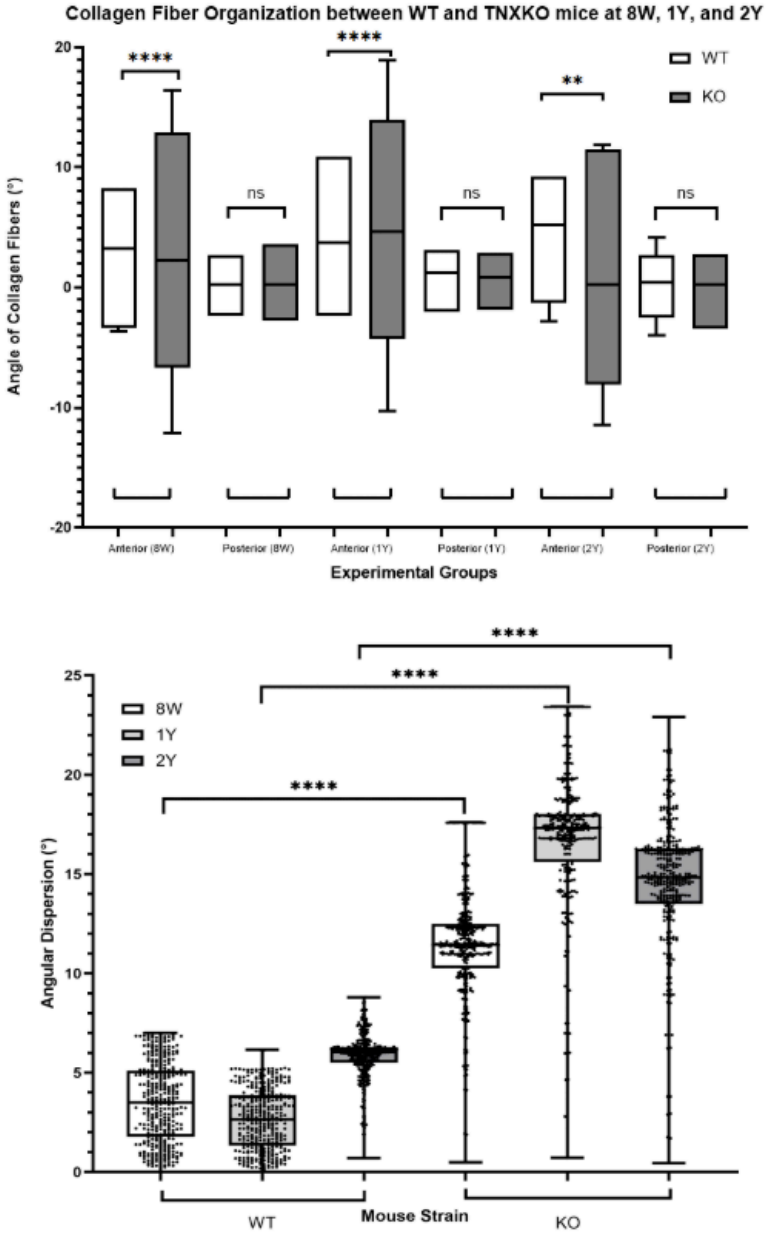

Figure 23: Collagen Organization Deviation from Norm

There was no significant difference (A) between WT and TNXKO in the posterior of the corneal stroma at any time point (8W, 1Y, and 2Y) but TNXKO collagen was much more disorganized than WT in the anterior stroma at 8W, 1Y, and 2Y ($p<0.0001$****, $p<0.0001$****, $p<0.01$** respectively). Angular dispersion between strains at each time point can be seen in (B). There was a significant difference when comparing between strains at each time point (($p<0.0001$****, $p<0.0001$****, $p<0.0001$****) but no significant difference within the group. The horizontal bar in each box plot represents the median.

Analysis

IHC

Keratocyte density values are consistent with those reported from other studies [107]. Keratocyte count comparison for the corneal buttons showed no significant differences with respect to time (8W vs 1Y vs 2Y, n = 2) and mouse strain (WT vs TNXKO).

SHG

Statistical results showed that there was a significant difference in the collagen organization (Fig 23, range in the lamellar angular direction) between WT and TNXKO mice in the anterior region of the stroma at 8W (****), 1Y (****), and 2Y (**). In the posterior region of the stroma, there were no significant differences between groups (WT vs TNXKO) or timepoint (8W, 1Y, and 2Y). The collagen lamellae in the TNXKO group appeared thicker than those in the WT but the differences were not measured but may be interesting to look at further. Angular dispersion of the collagen fibers (Fig 5B)

shows a significant difference between mouse strains at each time point but no difference within the strain.

Discussion

TNX plays an important role in regulating the corneal collagen organization and its presence maintains both transparency and biomechanics. Though the deficiency of TNX - as shown by corneal imaging of TNXKO mice corneas - does not seem to cause any change in the density of corneal keratocytes, it reveals an increasingly irregular and disorganized arrangement of collagen fibrils over time as well as a potential change in their thickness and density as compared to WT mice.

Supplementary

Information on the quantitative orientation and isotropy analysis performed by ImageJ's Directionality and OrientationJ plugins

First, to identify region of interest (ROI) on image

$$\langle f, g \rangle_w = \iint_{R^2} w(x,y) f(x,y) g(x,y) dx dy \qquad (1)$$

Here, $w(x, y) \geq 0$ is a weighting function that specifies an area of interest such as a normalized square window of user defined size (25 x 25 μm for this project) at location (x_0, y_0).

The directional derivative for the unit vector

$$\mathbf{u}_\theta = (\cos\theta, \sin\theta)$$

is

$$D_{\mathbf{u}_\theta} f(x,y) = \mathbf{u}_\theta{}^I \nabla f(x,y)$$

which is the gradient of the image. To find the direction **u** where the directional directive is maximized, we use the following equation

$$\mathbf{u}_\theta = \arg\max_{|u|=1} \|D_{\mathbf{u}} f\|_w^2 \qquad (2)$$

Manipulation of the inner-product yields the following:

$$\|D_{\mathbf{u}} f\|_w^2 = \left\langle \mathbf{u}^T \nabla f, \nabla f^T \mathbf{u} \right\rangle_w = \mathbf{u}^T \mathbf{J} \mathbf{u} \qquad (3)$$

Here, J (the structure tensor) is defined as

$$\mathbf{J} = \left\langle \nabla f, \nabla f^T \right\rangle_w = \begin{bmatrix} \langle f_x, f_x \rangle_w & \langle f_x, f_y \rangle_w \\ \langle f_x, f_y \rangle_w & \langle f_y, f_y \rangle_w \end{bmatrix}$$

After setting the derivative of the following equal to 0,

$$\mathbf{u}^T \mathbf{J} \mathbf{u} + 1 - \frac{\lambda}{2} \mathbf{u}^T \mathbf{u}$$

the function yields the following eigenvector equation:

$$\mathbf{Ju} = \lambda \mathbf{u}$$

From here, the first eigenvector of J gives the ROI's dominant direction while the second eigenvector provides the directional derivative. With this information, orientation and coherency can be obtained as follows:

$$\text{Orientation: } \theta = \frac{1}{2}\arctan\left(2\frac{\langle f_x, f_y\rangle_w}{\langle f_y, f_y\rangle_w - \langle f_x, f_x\rangle_w}\right)$$

$$\text{Coherency: } C = \frac{\lambda_{\max} - \lambda_{\min}}{\lambda_{\max} + \lambda_{\min}} = \frac{\sqrt{\left(\langle f_y, f_y\rangle_w - \langle f_x, f_x\rangle_w\right)^2 + 4\langle f_x, f_y\rangle_w}}{\langle f_x, f_x\rangle_w + \langle f_y, f_y\rangle_w}, C \in [0..1]$$

Here, C has a value of 1 when the image has a dominant direction and a value of 0 if the image is isotropic.

Chapter 5: Selective Photothermal Ablation (SPA)

Introduction

Meibomian gland dysfunction (MGD) is a chronic and diffuse condition affecting the meibomian glands. This condition is typically identified by obstructions in the terminal ducts and an alteration in the quantity or quality of glandular secretions. Obstructive MGD can lead to signs and symptoms of dry eye disease (DED) - a common disorder affecting more than 16 million adults in the US with an annual cost of $55.4 billion - and characterized by burning of the eye and blurry vision caused by tear film abnormalities, an increase in tear evaporation, and inflammation of the ocular surface. [110]

MGD-related dry eye is traditionally managed with techniques such as use of warm compresses, maintaining eyelid hygiene, meibomian gland expression, and pharmacotherapy. [111-113] Drug-based treatments for MGD exist and can be effective as well. However, patient compliance is required and long term efficacy and side effects are still unclear.

Recently, novel laser-based therapies involving intense pulsed light (IPL) and low-level light therapy (LLLT) have been shown to be effective in treating dry eye in the short term but lack standardization and cause indiscriminate tissue damage due to the wide spectral range being utilized. [114-118] A novel method, coined selective photothermolysis, has been in use in dermatology to treat acne by preferentially heating lipid and ablating skin sebaceous glands. With this approach, using a narrow bandwidth

laser tuned to a local absorption peak it should be possible to selectively separate the heating effect between the target gland and surrounding tissue. The purpose of this study was to introduce a novel narrow bandwidth FDA approved AviClear 1726 nm surgical laser for the feasibility study of selective photothermal ablation (SPA) for the treatment of dry eye disease. This laser would be able to selectively cause damage to the target with minimal injury to adjacent tissue.

Methods

SPA Laser System

The surgical laser system (Cutera Inc.) operates at 1726 nm and has tunable power capacity, variable pulse duration, and adjustable duty cycles. Laser pulses are delivered through a custom handpiece and pass through a glass slide to penetrate through the carefully flattened tissue which lays sandwiched between the slide and a metal block immersed in ice water. This setup (Fig 24) acts as a contact cooling system to prevent hyperthermal tissue damage.

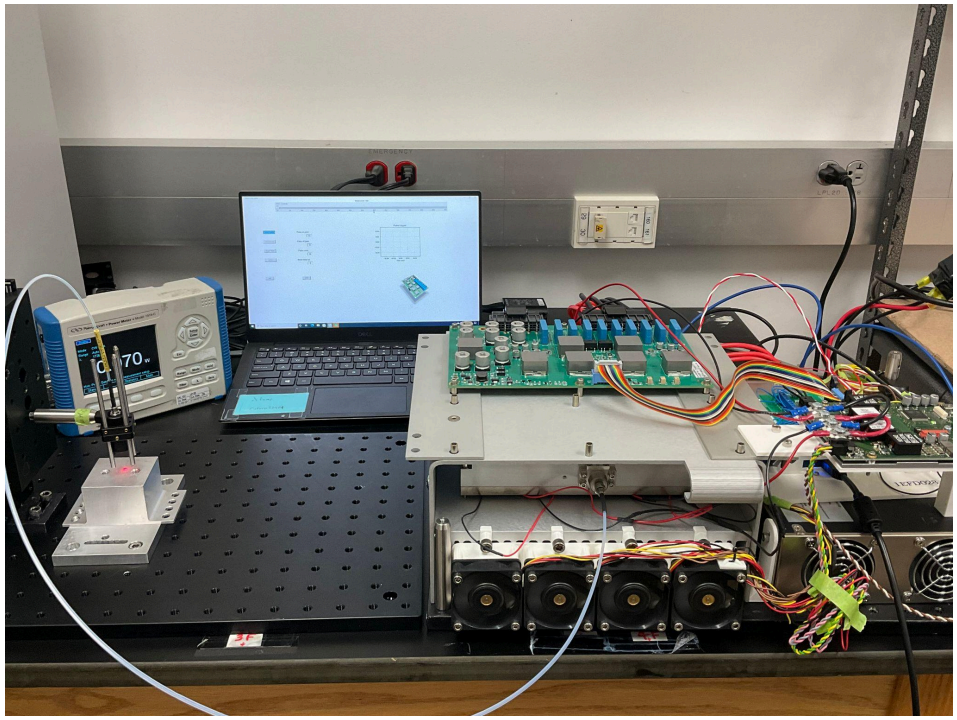

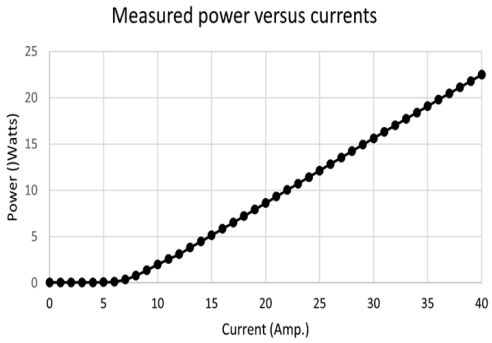

Figure 24: SPA Setup and Laser Calibration

The 1726 nm surgical laser (A) generated the coaxial visible red light which was used as a guide toward the desired meibomian glands beneath the conjunctiva and making them visible to the naked eye. Eyelid tissue is sandwiched between glass slide (B) and a metal block immersed in iced water to prevent hyperthermal tissue damage. A Newport 1918-C power meter was used to determine the average laser power (C) measured in air as a function of current (in amperes). High linearity is demonstrated when the current exceeds 8 amperes.

Eyelid Preparation for SPA Treatment

C57Bl/6 mice were sacrificed and upper eyelids were removed. The eyelid tissue was pre-cooled for 1 minute and then oriented so the conjunctiva faces up and can be exposed to the laser. After setting the laser variables - a 12 cycle periodic train with pulses of 10 ms on and 10 ms off (resultant 120 ms pulse) with a beam diameter of 500 um with varying energy levels of 3W to 9W, the laser was guided toward the desired meibomian gland with the aid of a coaxial visible red light. Each eyelid received one laser zap at the center of the tissue. A pre and post-meibography (Fig 25) image was taken and the tissue was fixed in 2% PFA for 24 hours immediately afterward.

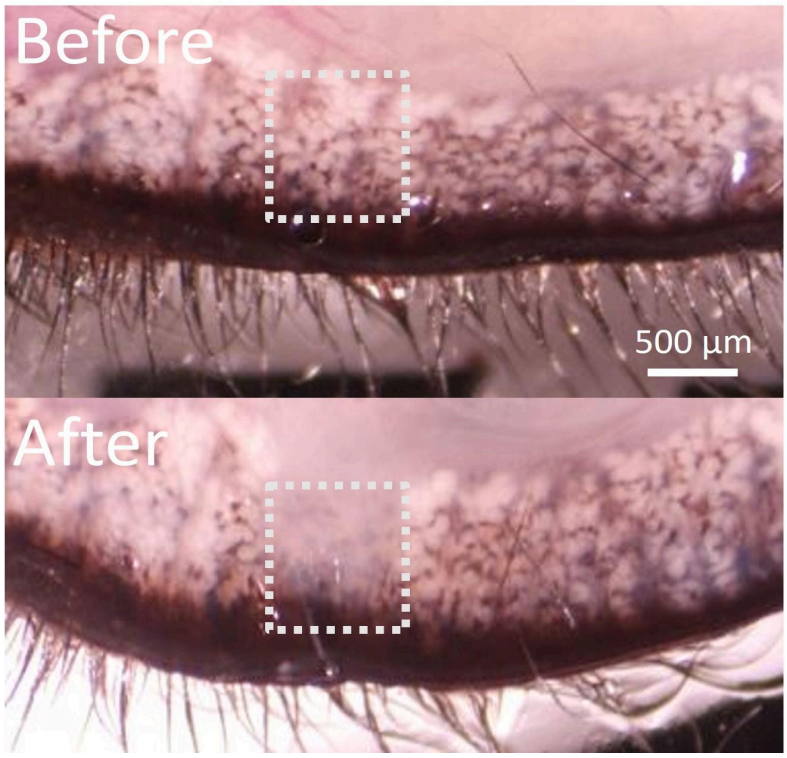

Figure 25: Eyelid Tissue Meibography Before and After Treatment

Using laser parameters of 500 µm beam diameter and 120 ms pulse duration, meibography images of eyelid tissue taken before and after SPA treatment illustrate selective targeting and removal of meibomian glands in the treated area without damaging the overlying conjunctiva.

Damage Assessment - H&E and IHC

Fixed samples were embedded in OCT and frozen in liquid nitrogen for subsequent cryosection. Tissues were stained with H&E to obtain histological results to evaluate laser damage. Images were taken using a standard light microscope (OLYMPUS BX60).

Results

The 1726 nm laser, operating above 5W, caused damage to the whole tissue (Fig 26). While operating at approximately 3-5W power however (Fig 27), the laser selectively heated the meibum while preserving the integrity of the conjunctiva on ex vivo mouse eyelids. Meibography images taken at this power revealed obliteration of the meibomian glands. H&E imaging and fluorescent imaging further confirmed the destruction of meibocytes and melting of meibum while the conjunctiva exhibited no discernible changes.

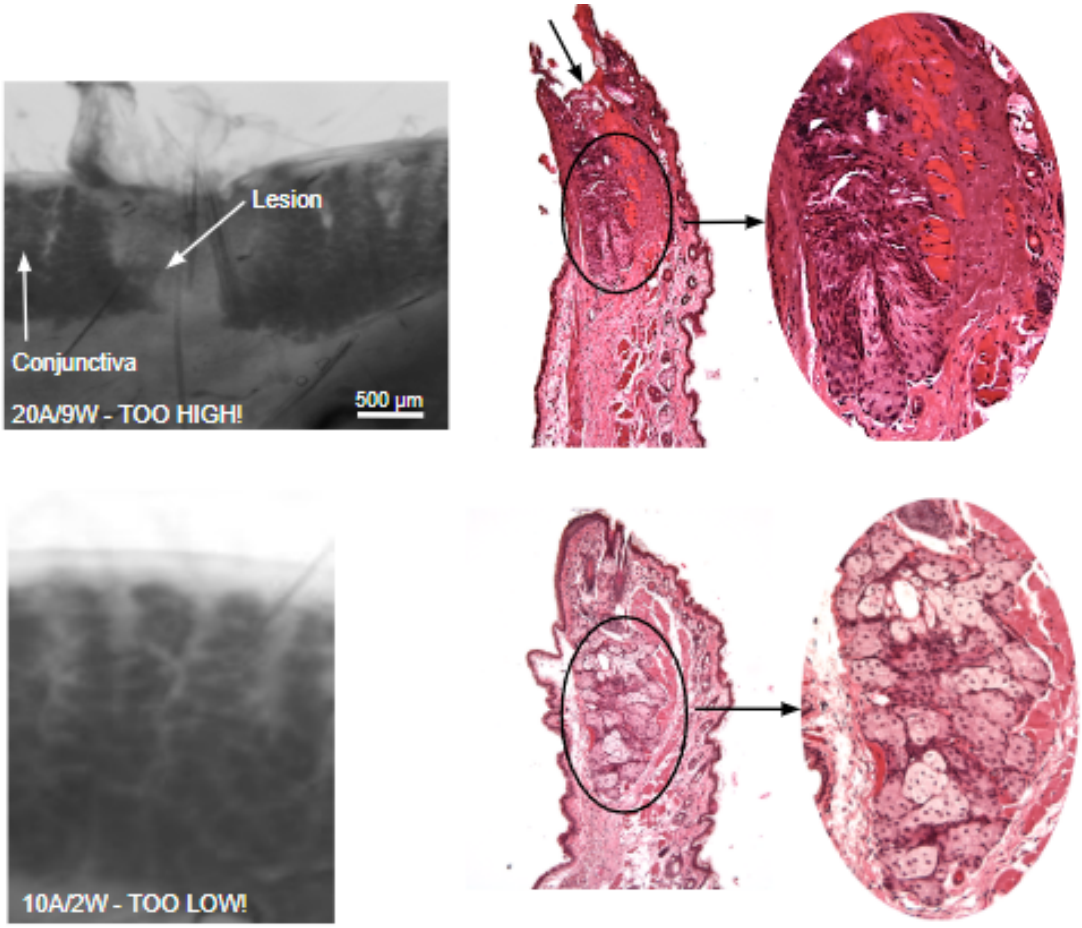

Figure 26: Meibography and H&E: High and Low

Images show differences between using high power/amperage vs low. High power (20A/9W) creates a lesion in the target area and melts the meibum but severely damages (arrow) the lid margin and conjunctiva. Low power (10A/2W) has no noticeable effect on the gland.

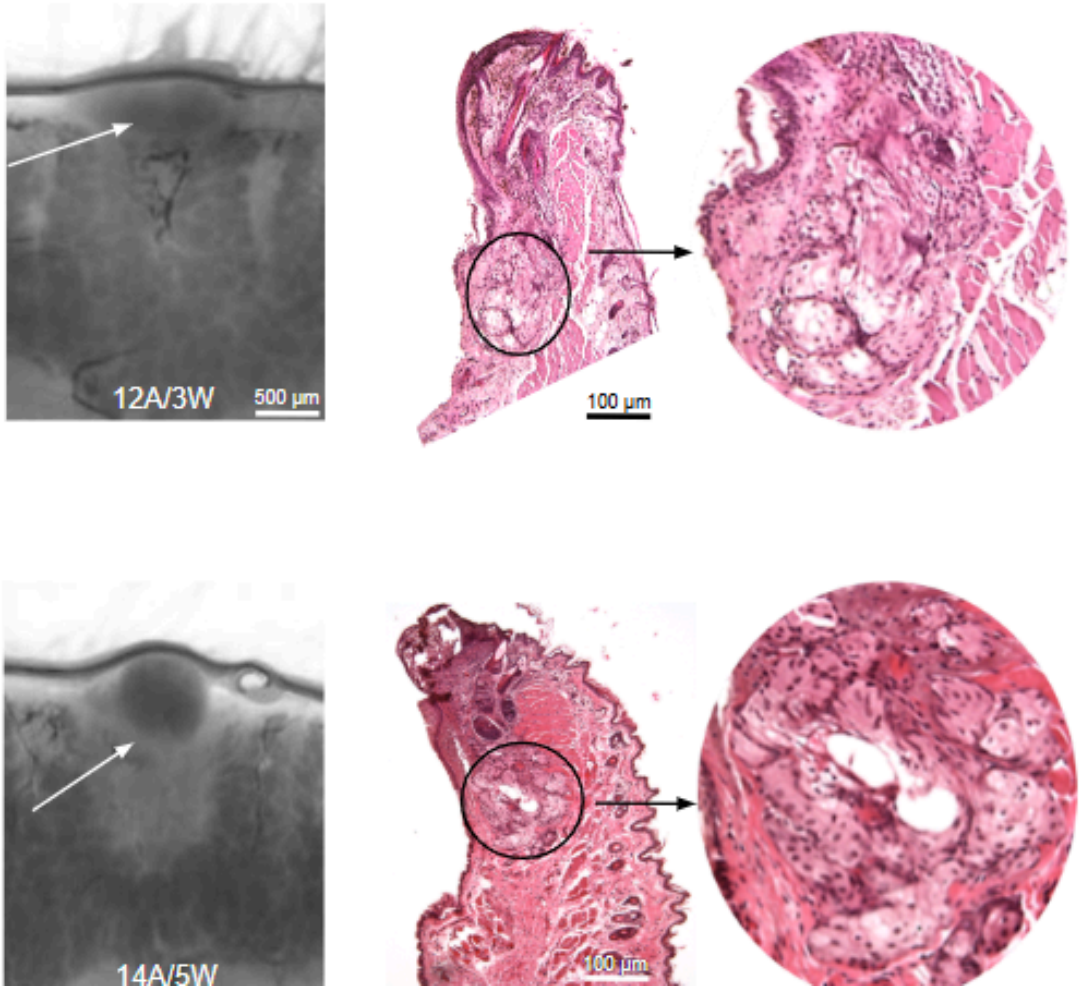

Figure 27: Meibography and H&E: 12-14A

Meibography shows lesions (arrows) being formed precisely on targeted glands. H&E reveals that the 12A/3W to 14A/5W range seems optimal in being able to melt the meibum in the glands while limiting or avoiding damage to the conjunctiva.

Discussion

SPA treatment exhibits selective treatment as demonstrated in pre- and post-treatment meibography images and further confirmed through H&E that reveal

meibomian gland shrinkage and selective meibum melting beneath the untouched overlying conjunctiva. By cooling the tissue before, during, and after treatment, we were able to maintain a safe range and mitigate hyperthermal damage to the tissue. In summary, SPA represents a promising novel treatment for MGD-related dry eye by selectively targeting meibomian glands with a narrowband 1726 nm in a controlled 3-5W range and melting the meibum while leaving the overlying tissue intact. We propose that this approach may be used to study meibomian gland regeneration and potential renewal.

Chapter 6: Conclusions and Ongoing Work

Conclusions

Crosslinking as a Treatment

Keratoconus and Post-LASIK Ectasia

Corneal collagen crosslinking was developed as a treatment for ectatic disorders such as Keratoconus and post-LASIK ectasia that weaken the collagen matrix. UVA CXL (Dresden Protocol) was recently approved as a standard and effective method to delay or treat the progression of these diseases. This method is able to triple the stiffness of human corneas with an equivalent increase in the elastic modulus. Unfortunately, despite this treatment's verified effectiveness, it lacks precision and requires the complete removal of the epithelial layer which results in patient pain, discomfort, and a delayed visual recovery.

Transepithelial Crosslinking - MC, Osmolarity, NLO, and Iontophoresis

Chapters 1-3 describe various methods to improve the existing UVA CXL procedure and offer promising alternatives.

In Chapter 1 we aimed to create a novel transepithelial method to match the efficacy of UVA CXL. NLO CXL - with its precise and controllable nature - enabled crosslinking at any stromal depth while also minimizing damage to the cornea and opens the possibility of a future topography-guided CXL. The use of FS-generated

epithelial microchannels also proved to significantly enhance the delivery of Rf into the stroma. Not only did microchannel-assisted delivery achieve stromal Rf concentrations of approximately 50% of those obtained through complete epithelial debridement and twice those obtained by competing BAK-enhanced delivery methods, but did so with minimal epithelial and stromal damage.

Chapter 2 explores our experimental design to test the safety and efficacy of MC UVA CXL with MC NLO CXL in addition to varying the osmolarity of the Rf solution to determine if we could further increase Rf stromal penetration as well as swell the cornea to the treatment-required 400 μm to broaden patient eligibility. Though our experiment with osmolarity was not significant, we were able to demonstrate that a combination of MC with NLO CXL resulted in a sufficient stromal Rf concentration to enable crosslinking while also avoiding epithelial damage and loss of corneal sensitivity in addition to significantly reduced anterior stromal damage and faster cellular recovery when compared to MC UVA CXL.

We next looked at various methods to further increase (passively or actively) Rf diffusion into the stroma while also increasing the treatment's efficacy. In Chapter 3, we paired Iontophoresis with MC and discovered a much higher rate of Rf diffusion which resulted in crosslinking at an equivalent level to UVA CXL - while significantly reducing the treatment time required from 30 minutes to 5 minutes. Future studies may incorporate this Iontophoresis + MC technique with our NLO treatment for an even faster and more precise CXL.

Tenascin-X KO

Tenascin-X is an important extracellular matrix glycoprotein that maintains the matrix integrity. A deficiency of TNX can lead to ocular conditions such as Keratoconus. In Chapter 4, we determined if TNX causes any changes in the corneal keratocyte density and stromal organization. Though there was no significant difference in the keratocyte density with respect to time and mouse strain, SHG revealed major changes in the collagen organization in TNXKO corneas - notably, an increasingly irregular and disorganized arrangement of collagen fibrils over time as well as a potential change in the fibril thickness as density.

Selective Photothermal Ablation

Meibomian gland dysfunction (MGD) is a chronic condition that affects the meibomian glands and results in obstruction of the terminal ducts and an alteration in meibum quantity and quality. This condition which usually leads to dry eye disease (DED), characterized by burning of the eye and blurry vision, affects millions of adults in the US. Though MGD-related DED can be somewhat managed by warm compresses, proper hygiene, and laser therapies such as IPL or LLLT, a better and safer method is required. In Chapter 5, we discuss our novel laser-based approach coined “Selective Photothermal Ablation” to selectively separate the heating effect between the target gland to melt the meibum while leaving the overlying tissue intact. Our results demonstrate that keeping our 1726 nm laser in the “sweet spot” range of 12-14A (3-5W)

results in meibomian gland shrinkage and selective meibum melting beneath the untouched overlying conjunctiva.

Bibliography

1. Wollensak G, Spoerl E, Seiler T. Riboflavin/ultraviolet-A-induced collagen crosslinking for the treatment of keratoconus. Am J Ophthalmol. 2003; 135: 620–627. [CrossRef] [PubMed]
2. Lim WK, Soh ZD, Choi HKY, Theng JTS. Epithelium-on photorefractive intrastromal cross-linking (PiXL) for reduction of low myopia. Clin Ophthalmol. 2017; 11: 1205–1211. [CrossRef] [PubMed]
3. Kamaev P, Freidman MD, Sherr E, Muller D. Photochemical kinetics of corneal cross-linking with riboflavin. Invest Ophthalmol Vis Sci. 2012; 53: 2360–2367. [CrossRef] [PubMed]
4. Raiskup F, Spoerl E. Corneal crosslinking with riboflavin and ultraviolet A: I. Principles. Ocul Surf. 2013; 11: 65–74. [CrossRef] [PubMed].
5. Bradford SM, Brown DJ, Juhasz T, Mikula E, Jester JV. Nonlinear optical corneal collagen crosslinking of ex vivo rabbit eyes. J Cataract Refract Surg. 2016; 42: 1660–1665. [CrossRef] [PubMed]
6. Bradford SM, Mikula ER, Chai D, Brown DJ, Juhasz T, Jester JV. Custom built nonlinear optical crosslinking (NLO CXL) device capable of producing mechanical stiffening in ex vivo rabbit corneas. Biomed Opt Express. 2017; 8: 4788–4797. [CrossRef] [PubMed]
7. Wollensak G, Iomdina E. Long-term biomechanical properties of rabbit cornea after photodynamic collagen crosslinking. Acta Ophthalmol. 2009; 87: 48–51. [CrossRef] [PubMed]
8. De Bernardo M, Capasso L, Lanza M, et al. Long-term results of corneal collagen crosslinking for progressive keratoconus. J Optom. 2015; 8: 180–186. [CrossRef] [PubMed]
9. Elling M, Kersten-Gomez I, Dick HB. Photorefractive intrastromal corneal crosslinking for the treatment of myopic refractive errors: Six-month interim findings. J Cataract Refract Surg. 2017; 43: 789–795. [CrossRef] [PubMed]
10. Hersh PS, et al. United States multicenter clinical trial of corneal collagen crosslinking for keratoconus treatment. Ophthalmology. 2017; 124: 1259–1270. [CrossRef] [PubMed]
11. Kanellopoulos AJ, Asimellis G. Combined laser in situ keratomileusis and prophylactic high-fluence corneal collagen crosslinking for high myopia: two-year safety and efficacy. J Cataract Refract Surg, 2015; 41: 1426–1433. [CrossRef] [PubMed]
12. Malik S, Humayun S, Nayyar S, Ishaq M. Determining the efficacy of corneal crosslinking in progressive keratoconus. Pak J Med Sci. 2017; 33: 389–392. [PubMed]

13. Raiskup-Wolf F, Hoyer A, Spoerl E, Pillunat LE. Collagen crosslinking with riboflavin and ultraviolet-A light in keratoconus: long-term results. J Cataract Refract Surg. 2008; 34: 796–801. [CrossRef] [PubMed]
14. Shalchi Z, Wang X, Nanavaty MA. Safety and efficacy of epithelium removal and transepithelial corneal collagen crosslinking for keratoconus. Eye (Lond). 2015; 29: 15–29. [CrossRef] [PubMed]
15. Vinciguerra P, Albe E, Trazza S, Seiler T, Epstein D. Intraoperative and postoperative effects of corneal collagen cross-linking on progressive keratoconus. Arch Ophthalmol. 2009; 127: 1258–1265. [CrossRef] [PubMed]
16. Wollensak G, Spoerl E, Wilsch M, Seiler T. Endothelial cell damage after riboflavin-ultraviolet-A treatment in the rabbit. J Cataract Refract Surg. 2003; 29: 1786–1790. [CrossRef] [PubMed]
17. Seiler TG, Fischinger I, Koller T, Zapp D, Frueh BE, Seiler T. Customized corneal cross-linking: one-year results. Am J Ophthalmol. 2016; 166: 14–21. [CrossRef] [PubMed]
18. Koller T, Mrochen M, Seiler T. Complication and failure rates after corneal crosslinking. J Cataract Refract Surg. 2009; 35: 1358–1362. [CrossRef] [PubMed]
19. Gore DM, O'Brart D, French P, Dunsby C, Allan BD. Transepithelial riboflavin absorption in an ex vivo rabbit corneal model. Invest Ophthalmol Vis Sci. 2015; 56: 5006–5011. [CrossRef] [PubMed]
20. Hayes S, Morgan SR, O'Brart DP, O'Brart N, Meek KM. A study of stromal riboflavin absorption in ex vivo porcine corneas using new and existing delivery protocols for corneal cross-linking. Acta Ophthalmol. 2016; 94: e109–e117. [CrossRef] [PubMed]
21. Akbar B, Intisar-Ul-Kaq R, Ishaq M, Arzoo S, Siddique K. Transepithelial corneal crosslinking in treatment of progressive keratoconus: 12 months' clinical results. Pak J Med Sci. 2017; 33: 570–575. [CrossRef] [PubMed]
22. Aldahlawi NH, Hayes S, O'Brart DPS, O'Brart ND, Meek KM. An investigation into corneal enzymatic resistance following epithelium-off and epithelium-on corneal cross-linking protocols. Exp Eye Res. 2016; 153: 141–151. [CrossRef] [PubMed]
23. Chow SSW, Chan TCY, Wong IYH, Fan MCY, Lai JSM, Ng ALK. Early epithelial complications of accelerated trans-epithelial corneal crosslinking in treatment of keratoconus: a case series. Int Ophthalmol. 2018; 38: 2635–2638. [CrossRef] [PubMed]
24. Ostacolo C, Caruso C, Tronino D, et al. Enhancement of corneal permeation of riboflavin-5'-phosphate through vitamin E TPGS: a promising approach in corneal trans-epithelial cross linking treatment. Int J Pharm. 2013; 440: 148–153. [CrossRef] [PubMed]
25. Koc M, Bostanci B, Demirel OO, et al. The effect of ascorbic acid (vitamin C) on transepithelial corneal cross-linking in rabbits. J Ocul Pharmacol Ther. 2017; 33: 525–529. [CrossRef] [PubMed]

26. Cassagne M, Laurent C, Rodrigues M, et al. Iontophoresis transcorneal delivery technique for transepithelial corneal collagen crosslinking with riboflavin in a rabbit model. Invest Ophthalmol Vis Sci. 2016; 57: 594–603. [CrossRef] [PubMed]
27. Mastropasqua L, Nubile M, Calienno R, et al. Corneal cross-linking: intrastromal riboflavin concentration in iontophoresis-assisted imbibition versus traditional and transepithelial techniques. Am J Ophthalmol. 2014; 157: 623–630, e1. [CrossRef] [PubMed]
28. Gore DM, O'Brart DP, French P, Dunsby C, Allan BD. A comparison of different corneal iontophoresis protocols for promoting transepithelial riboflavin penetration. Invest Ophthalmol Vis Sci. 2015; 56: 7908–7914. [CrossRef] [PubMed]
29. Vinciguerra P, Mencucci R, Romano V, et al. Imaging mass spectrometry by matrix-assisted laser desorption/ionization and stress-strain measurements in iontophoresis transepithelial corneal collagen cross-linking. Biomed Res Int. 2014; 2014: 404587. [CrossRef] [PubMed]
30. Bottos KM, Schor P, Dreyfuss JL, Nader HB, Chamon W. Effect of corneal epithelium on ultraviolet-A and riboflavin absorption. Arq Bras Oftalmol. 2011; 74: 348–351. [CrossRef] [PubMed]
31. Kobashi H, Rong SS, Ciolino JB. Transepithelial versus epithelium-off corneal crosslinking for corneal ectasia. J Cataract Refract Surg. 2018; 44: 1507–1516. [CrossRef] [PubMed]
32. Rush SW, Rush RB. Epithelium-off versus transepithelial corneal collagen crosslinking for progressive corneal ectasia: a randomised and controlled trial. Br J Ophthalmol. 2017; 101: 503–508. [CrossRef] [PubMed]
33. Rasmussen CA, Kaufman PL, Kiland JA. Benzalkonium chloride and glaucoma. J Ocul Pharmacol Ther. 2014; 30: 163–169. [CrossRef] [PubMed]
34. Chen W, Zhang Z, Hu J, et al. Changes in rabbit corneal innervation induced by the topical application of benzalkonium chloride. Cornea. 2013; 32: 1599–1606. [CrossRef] [PubMed]
35. Bradford SM, Mikula ER, Juhasz R, Brown DJ, Jester JV. Collagen fiber crimping following in vivo UVA-induced corneal crosslinking. Exp Eye Res. 2018; 177: 173–180. [CrossRef] [PubMed]
36. Cui L, Huxlin KR, Xu L, MacRae S, Knox WH. High-resolution, noninvasive, two-photon fluorescence measurement of molecular concentrations in corneal tissue. Invest Ophthalmol Vis Sci. 2011; 52: 2556–2564. [CrossRef] [PubMed]
37. Lebrun S, Xie Y, Chavez S, Chan R, Jester JV. An in vitro depth of injury prediction model for a histopathologic classification of EPA and GHS eye irritants. Toxicol In Vitro. 2019; 61: 104628. [CrossRef] [PubMed]
38. Rubinfeld RS, Stulting RD, Gum GG, Talamo JH. Quantitative analysis of corneal stromal riboflavin concentration without epithelial removal. J Cataract Refract Surg. 2018; 44: 237–242. [CrossRef] [PubMed]

39. Lombardo G, Serrao S, Lombardo M. Comparison between standard and transepithelial corneal crosslinking using a theranostic UV-A device. Graefes Arch Clin Exp Ophthalmol. 2020; 258: 829–834. [PubMed]
40. Hollhumer R, Watson S, Beckingsale P. Persistent epithelial defects and corneal opacity after collagen cross-linking with substitution of dextran (T-500) with dextran sulfate in compounded topical riboflavin. *Cornea*. 2017; 36: 382–385. [CrossRef] [PubMed]
41. Al-Qarni A, AlHarbi M. Herpetic keratitis after corneal collagen cross-linking with riboflavin and ultraviolet-A for keratoconus. *Middle East Afr J Ophthalmol*. 2015; 22: 389–392. [CrossRef] [PubMed]
42. Perez-Santonja JJ, Artola A, Javaloy J, Alio JL, Abad JL. Microbial keratitis after corneal collagen crosslinking. *J Cataract Refract Surg*. 2009; 35: 1138–1140. [CrossRef] [PubMed]
43. Wollensak G, Iomdina E, Dittert DD, Herbst H. Wound healing in the rabbit cornea after corneal collagen cross-linking with riboflavin and UVA. *Cornea*. 2007; 26: 600–605. [CrossRef] [PubMed]
44. O'Brart DP. Corneal collagen cross-linking: a review. *J Optom*. 2014; 7: 113–124. [CrossRef] [PubMed]
45. Lombardo G, Micali NL, Villari V, et al. Assessment of stromal riboflavin concentration-depth profile in nanotechnology-based transepithelial corneal crosslinking. *J Cataract Refract Surg*. 2017; 43: 680–686. [CrossRef] [PubMed]
46. Bradford S, Mikula E, Xie Y, Juhasz T, Brown DJ, Jester JV. Enhanced transepithelial riboflavin delivery using femtosecond laser-machined epithelial microchannels. *Transl Vis Sci Technol*. 2020; 9: 1. [CrossRef] [PubMed]
47. Taneri S, Oehler S, Lytle G, Dick HB. Evaluation of epithelial integrity with various transepithelial corneal cross-linking protocols for treatment of keratoconus. *J Ophthalmol*. 2014; 2014: 614380. [PubMed]
48. Armstrong BK, Lin MP, Ford MR, et al. Biological and biomechanical responses to traditional epithelium-off and transepithelial riboflavin-UVA CXL techniques in rabbits. *J Refract Surg*. 2013; 29: 332–341. [CrossRef] [PubMed]
49. Torricelli AA, Ford MR, Singh V, Santhiago MR, Dupps WJ, Jr, Wilson SE. BAC-EDTA transepithelial riboflavin-UVA crosslinking has greater biomechanical stiffening effect than standard epithelium-off in rabbit corneas. *Exp Eye Res*. 2014; 125: 114–117. [CrossRef] [PubMed]
50. Bradford S, Mikula E, Kim SW, et al. Nonlinear optical corneal crosslinking, mechanical stiffening, and corneal flattening using amplified femtosecond pulses. *Transl Vis Sci Technol*. 2019; 8: 35. [CrossRef] [PubMed]
51. Bankhead P, Loughrey MB, Fernandez JA, et al. QuPath: open source software for digital pathology image analysis. *Sci Rep*. 2017; 7: 16878. [CrossRef] [PubMed]
52. Morgan SR, O'Brart DPS, Huang J, Meek KM, Hayes S. An in vitro investigation into the impact of corneal rinsing on riboflavin/UVA corneal cross-linking. *Eye Vis (Lond)*. 2024; 11: 8. [CrossRef] [PubMed]
53. Xia Y, Chai X, Zhou C, Ren Q. Corneal nerve morphology and sensitivity changes after ultraviolet A/riboflavin treatment. *Exp Eye Res*. 2011; 93: 541–547. [CrossRef] [PubMed]

54. Mazzotta C, Hafezi F, Kymionis G, et al. In vivo confocal microscopy after corneal collagen crosslinking. *Ocul Surf*. 2015; 13: 298–314. [CrossRef] [PubMed]
55. Brosh K, Rozenman Y. Chemical burn-induced stromal demarcation line. *Cornea*. 2016; 35: 286–288. [CrossRef] [PubMed]
56. Niazi S, Gatzioufas Z, Doroodgar F, et al. Keratoconus: exploring fundamentals and future perspectives - a comprehensive systematic review. *Ther Adv Ophthalmol*. 2024; 16: 25158414241232258. [PubMed]
57. Moshirfar M, Tukan AN, Bundogji N, et al. Ectasia after corneal refractive surgery: a systematic review. *Ophthalmol Ther*. 2021; 10: 753–776. [CrossRef] [PubMed]
58. Galvis V, Tello A, Carreno NI, et al. Corneal cross-linking (with a partial deepithelization) in keratoconus with five years of follow-up. *Ophthalmol Eye Dis*. 2016; 8: 17–21. [CrossRef] [PubMed]
59. Galvis V, Tello A, Barrera R, Nino CA. Inflammation in keratoconus. *Cornea*. 2015; 34: e22–e23. [CrossRef] [PubMed]
60. Rabinowitz YS, Galvis V, Tello A, Rueda D, Garcia JD. Genetics vs chronic corneal mechanical trauma in the etiology of keratoconus. *Exp Eye Res*. 2021; 202: 108328. [CrossRef] [PubMed]
61. Gatinel D, Galvis V, Tello A, et al. Obstructive sleep apnea-hypopnea syndrome and keratoconus: an epiphenomenon related to sleep position? *Cornea*. 2020; 39: e11–e12. [CrossRef] [PubMed]
62. Vega A, Alio JL. Criteria for patient selection and indication for intracorneal ring segments in keratoconus. *Eye Vis (Lond)*. 2024; 11: 13. [CrossRef] [PubMed]
63. Al Bdour M, Abu-Ameerh M, Gharaibeh A, et al. Intrastromal corneal ring segments for keratoconus patients: up to 12 years follow up. *Int Ophthalmol*. 2024; 44: 50. [CrossRef] [PubMed]
64. Sarma P, Kaur H, Hafezi F, et al. Short- and long-term safety and efficacy of corneal collagen cross-linking in progressive keratoconus: a systematic review and meta-analysis of randomized controlled trials. *Taiwan J Ophthalmol*. 2023; 13: 191–202. [CrossRef] [PubMed]
65. Riau AK, Htoon HM, Alio Del Barrio JL, et al. Femtosecond laser-assisted stromal keratophakia for keratoconus: a systemic review and meta-analysis. *Int Ophthalmol*. 2021; 41: 1965–1979. [CrossRef] [PubMed]
66. Doroodgar F, Jabbarvand M, Niazi S, et al. Customized stromal lenticule implantation for keratoconus. *J Refract Surg*. 2020; 36: 786–794. [CrossRef] [PubMed]
67. Estrada-Mata AG, Benedetti Sandner M, Garcia de Oteyza G, et al. Bowman layer transplantation with stromal inclusion using femtosecond laser: 3-year results [published online ahead of print July 10, 2024]. *Cornea*, doi:10.1097/ICO.0000000000003620.
68. Jacob S, Agarwal A, Awwad ST, Mazzotta C, Parashar P, Jambulingam S. Customized corneal allogenic intrastromal ring segments (CAIRS) for keratoconus with decentered asymmetric cone. *Indian J Ophthalmol*. 2023; 71: 3723–3729. [CrossRef] [PubMed]
69. Mazzotta C, Balestrazzi A, Traversi C, et al. Treatment of progressive keratoconus by riboflavin-UVA-induced cross-linking of corneal collagen:

ultrastructural analysis by Heidelberg Retinal Tomograph II in vivo confocal microscopy in humans. *Cornea*. 2007; 26: 390–397. [CrossRef] [PubMed]
70. Spoerl E, Mroehen M, Sliney D, Trokel S, Seiler T. Safety of UVA-riboflavin cross-linking of the cornea. *Cornea*. 2007; 26: 385–389. [CrossRef] [PubMed]
71. Chai D, Gaster RN, Roizenblatt R, Juhasz T, Brown DJ, Jester JV. Quantitative assessment of UVA-riboflavin corneal cross-linking using nonlinear optical microscopy. *Invest Ophthalmol Vis Sci*. 2011; 52: 4231–4238. [CrossRef] [PubMed]
72. Spoerl E, Raiskup F, Kampik D, Geerling G. Correlation between UV absorption and riboflavin concentration in different depths of the cornea in CXL. *Curr Eye Res*. 2010; 35: 1040–1041; author reply 1042–1043. [CrossRef] [PubMed]
73. Schilde T, Kohlhaas M, Spoerl E, Pillunat LE. Enzymatic evidence of the depth dependence of stiffening on riboflavin/UVA treated corneas [in German]. *Ophthalmologe*. 2008; 105: 165–169. [CrossRef] [PubMed]
74. Spadea L, Salvatore S, Paroli MP, Vingolo EM. Recovery of corneal sensitivity after collagen crosslinking with and without epithelial debridement in eyes with keratoconus. *J Cataract Refract Surg*. 2015; 41: 527–532. [CrossRef] [PubMed]
75. Cagil N, Sarac O, Cakmak HB, Can G, Can E. Mechanical epithelial removal followed by corneal collagen crosslinking in progressive keratoconus: short-term complications. *J Cataract Refract Surg*. 2015; 41: 1730–1737. [CrossRef] [PubMed]
76. Razmjoo H, Rahimi B, Kharraji M, Koosha N, Peyman A. Corneal haze and visual outcome after collagen crosslinking for keratoconus: a comparison between total epithelium off and partial epithelial removal methods. *Adv Biomed Res*. 2014; 3: 221. [PubMed]
77. Hashemi H, Miraftab M, Hafezi F, Asgari S. Matched comparison study of total and partial epithelium removal in corneal cross-linking. *J Refract Surg*. 2015; 31: 110–115. [CrossRef] [PubMed]
78. Rechichi M, Daya S, Scorcia V, Meduri A, Scorcia G. Epithelial-disruption collagen crosslinking for keratoconus: one-year results. *J Cataract Refract Surg*. 2013; 39: 1171–1178. [CrossRef] [PubMed]
79. Bakke EF, Stojanovic A, Chen X, Drolsum L. Penetration of riboflavin and postoperative pain in corneal collagen crosslinking: excimer laser superficial versus mechanical full-thickness epithelial removal. *J Cataract Refract Surg*. 2009; 35: 1363–1366. [CrossRef] [PubMed]
80. Akbar B, Intisar-Ul-Haq R, Ishaq M, Fawad A, Arzoo S, Siddique K. Comparison of transepithelial corneal crosslinking with epithelium-off crosslinking (epithelium-off CXL) in adult Pakistani population with progressive keratoconus. *Taiwan J Ophthalmol*. 2017; 7: 185–190. [CrossRef] [PubMed]
81. Boxer Wachler BS, Pinelli R, Ertan A, Chan CC. Safety and efficacy of transepithelial crosslinking (C3-R/CXL). *J Cataract Refract Surg*. 2010; 36: 186–188; author reply 188–189. [CrossRef] [PubMed]
82. Bouheraoua N, Jouve L, Borderie V, Laroche L. Three different protocols of corneal collagen crosslinking in keratoconus: conventional, accelerated and iontophoresis. *J Vis Exp*. 2015; 105: 53119.

83. Li N, Peng X, Fan Z, Xia Y. Iontophoretic delivery of riboflavin into the rabbit cornea: a primary study. *Eye Sci*. 2014; 29: 30–35. [PubMed]
84. Wan KH, Ip CKY, Kua WN, et al. Transepithelial corneal collagen cross-linking using iontophoresis versus the Dresden protocol in progressive keratoconus: a meta-analysis. *Clin Exp Ophthalmol*. 2021; 49: 228–241. [CrossRef] [PubMed]
85. Bikbova G, Bikbov M. Transepithelial corneal collagen cross-linking by iontophoresis of riboflavin. *Acta Ophthalmol*. 2014; 92: E30–E34. [CrossRef] [PubMed]
86. Jia HZ, Pang X, Fan ZJ, Li N, Li G, Peng XJ. Iontophoresis-assisted corneal crosslinking using 0.1% riboflavin for progressive keratoconus. *Int J Ophthalmol-Chi*. 2017; 10: 717–722.
87. Halhal M, Renard G, Bejjani RA, Behar-Cohen F. Corneal graft rejection and corticoid iontophoresis: 3 case reports. *J Fr Ophtalmol*. 2003; 26: 391–395. [PubMed]
88. Halhal M, Renard G, Courtois Y, BenEzra D, Behar-Cohen F. Iontophoresis: from the lab to the bed side. *Exp Eye Res*. 2004; 78: 751–757. [CrossRef] [PubMed]
89. Souza JG, Dias K, Silva SA, et al. Transcorneal iontophoresis of dendrimers: PAMAM corneal penetration and dexamethasone delivery. *J Control Release*. 2015; 200: 115–124. [CrossRef] [PubMed]
90. Costello CT, Jeske AH. Iontophoresis - applications in transdermal medication delivery. *Phys Ther*. 1995; 75: 554–563. [CrossRef] [PubMed]
91. Keeler R, Singh AD, Dua HS. Carving the cornea: the von Hippel trephine. *Br J Ophthalmol*. 2009; 93: 847. [PubMed]
92. Vinciguerra P, Rosetta P, Legrottaglie EF, et al. Iontophoresis CXL with and without epithelial debridement versus standard CXL: 2-year clinical results of a prospective clinical study. *J Refract Surg*. 2019; 35: 184–190. [CrossRef] [PubMed]
93. Jouve L, Borderie V, Temstet C, et al. Corneal collagen crosslinking in keratoconus. *J Fr Ophtalmol*. 2015; 38: 445–462. [CrossRef] [PubMed]
94. Bikbova G, Bikbov M. Standard corneal collagen crosslinking versus transepithelial iontophoresis-assisted corneal crosslinking, 24 months follow-up: randomized control trial. *Acta Ophthalmol*. 2016; 94: E600–E606. [CrossRef] [PubMed]
95. Kalkanci A, Yesilirmak N, Ozdemir HB, et al. Impact of iontophoresis and PACK-CXL corneal concentrations of antifungals in an in vivo model. *Cornea*. 2018; 37: 1463–1467. [CrossRef] [PubMed]
96. Bradford S, Mikula E, Juhasz T, Brown DJ, Jester JV. Nonlinear optical crosslinking (NLO CXL) for correcting refractive errors. *Exp Eye Res*. 2020; 199: 108199. [CrossRef] [PubMed]
97. Bikbova G, Khalimov A, Kazakbaeva G, Bikbov M. Molecular mechanisms of corneal collagen crosslinking. *Invest Ophthalmol Vis Sci*. 2018; 59: 522.
98. Brekelmans J, Dickman MM, Verma S, et al. Excimer laser-assisted corneal epithelial pattern ablation for corneal cross-linking. *Acta Ophthalmol*. 2022; 100: 422–430. [CrossRef] [PubMed]

99. Bradford S, Joshi R, Luo S, et al. In vivo femtosecond laser machined transepithelial nonlinear optical corneal crosslinking compared to ultraviolet corneal crosslinking. *Transl Vis Sci Technol*. 2024; 13: 9. [CrossRef] [PubMed]
100. Di Y, Wang J, Li Y, Jiang Y. Comparison of standard and transepithelial corneal cross-linking for the treatment of keratoconus: a meta-analysis. *J Ophthalmol*. 2021; 2021: 6679770. [CrossRef] [PubMed]
101. Li N, Fan Z, Peng X. A histological examination of corneal epithelium after iontophoresis with different riboflavin solutions. *Chin Med J (Engl)*. 2022; 135: 753–755. [CrossRef] [PubMed]
102. Rossi S, Santamaria C, Boccia R, et al. Standard, transepithelial and iontophoresis corneal cross-linking: clinical analysis of three surgical techniques. *Int Ophthalmol*. 2018; 38: 2585–2592. [CrossRef] [PubMed]
103. Gupta P, Anyama B, Edward K, et al. Depth resolved differences after corneal crosslinking with and without epithelial debridement using multimodal imaging. *Transl Vis Sci Technol*. 2014; 3: 5. [CrossRef]
104. Ozmen MC, Hondur A, Yilmaz G, Bilgihan K, Hasanreisoglu B. A histological study of rabbit corneas after transepithelial corneal crosslinking using partial epithelial photoablation or ethanol treatment. *Int J Ophthalmol*. 2014; 7: 959–963. [PubMed]
105. Sumioka, T., Iwanishi, H., Okada, Y., Miyajima, M., Ichikawa, K., Reinach, P. S., Matsumoto, K., & Saika, S. (2021). Impairment of corneal epithelial wound healing is association with increased neutrophil infiltration and reactive oxygen species activation in tenascin X-deficient mice. Laboratory Investigation, 101(6), 690–700. https://doi.org/10.1038/s41374-021-00576-8
106. Sumioka, T., Matsumoto, K., Reinach, P. S., & Saika, S. (2023). Tenascins and osteopontin in biological response in cornea. The Ocular Surface, 29, 131–149. https://doi.org/10.1016/j.jtos.2023.05.005
107. Jeang, L., Cha, B. J., Birk, D. E., & Espana, E. M. (2020). Endothelial–stromal communication in murine and human corneas. *The Anatomical Record*, *303*(6), 1717–1726. https://doi.org/10.1002/ar.24393
108. Elena Koudouna, Eric Mikula, Donald J. Brown, Robert D. Young, Andrew J. Quantock, James V. Jester, Cell regulation of collagen fibril macrostructure during corneal morphogenesis, Acta Biomaterialia, Volume 79, 2018, Pages 96-112, ISSN 1742-7061, https://doi.org/10.1016/j.actbio.2018.08.017.
109. Winkler, M., Chai, D., Kriling, S., Nien, C. J., Brown, D. J., Jester, B., Juhasz, T., & Jester, J. V. (2011). Nonlinear Optical Macroscopic Assessment of 3-D corneal collagen organization and axial biomechanics. Investigative Opthalmology & Visual Science, 52(12), 8818. https://doi.org/10.1167/iovs.11-8070
110. Tomlinson A, Bron AJ, Korb DR, Amano S, Paugh JR, Pearce EI, et al. The international workshop on meibomian gland dysfunction: report of the diagnosis subcommittee. Invest Ophthalmol Vis Sci. 2011;52:2006-49.
111. Kojima T, Dogru M, Kawashima M, Nakamura S, Tsubota K. Advances in the diagnosis and treatment of dry eye. Prog Retin Eye Res. 2020;78

112. Kaido M, Ibrahim OM, Kawashima M, Ishida R, Sato EA, Tsubota K. Eyelid cleansing with ointment for obstructive meibomian gland dysfunction. Jpn J Ophthalmol. 2017;61:124-30
113. Goto E, Monden Y, Takano Y, Mori A, Shimmura S, Shimazaki J, et al. Treatment of non-inflamed obstructive meibomian gland dysfunction by an infrared warm compression device. Br J Ophthalmol. 2002;86:1403-7
114. Park Y, Kim H, Kim S, Cho KJ. Effect of low-level light therapy in patients with dry eye: a prospective, randomized, observer-masked trial. Sci Rep. 2022;12:3575
115. Markoulli M, Chandramohan N, Papas EB. Photobiomodulation (low-level light therapy) and dry eye disease. Clin Exp Optom. 2021;104:561-6
116. Perez-Silguero MA, Perez-Silguero D, Rivero-Santana A, Bernal-Blasco MI, Encinas-Pisa P. Combined Intense Pulsed Light and Low-Level Light Therapy for the Treatment of Dry Eye: A Retrospective Before-After Study with One-Year Follow-Up. Clin Ophthalmol. 2021;15:2133-40.
117. Di Marino M, Conigliaro P, Aiello F, Valeri C, Giannini C, Mancino R, et al. Combined Low-Level Light Therapy and Intense Pulsed Light Therapy for the Treatment of Dry Eye in Patients with Sjogren's Syndrome. J Ophthalmol. 2021;2021:2023246.
118. Scopelliti MG, Kothare A, Karavitis M. A novel 1726-nm laser system for safe and effective treatment of acne vulgaris. Lasers Med Sci. 2022;37:3639-47.